Study of Structural Properties of $MnO_2 - Fe_2O_3$ Doped Bioactive Silicate Glasses

A Dissertation for

PHY-651 Discipline Specific Dissertation
Credits: 16
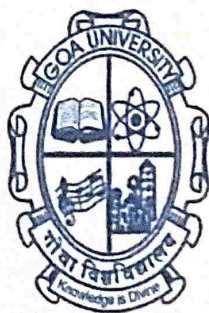Submitted in partial fulfillment of Masters Degree

M.Sc. in Physics
Goa University
In the subject of Physics

by

Vishvam Umanth Naik

22P0430046
ABC ID : 235-722-826-366
201911568

Under the Supervision of
Dr.Reshma Raut Dessai

School of Physical and Applied Sciences
Physics Discipline

Goa University
May 2024

Seal of the School

Examined by:

DECLARATION BY STUDENT

I hereby declare that the data presented in this Dissertation report entitled, "Study of Structural Properties of $MnO_2 - Fe_2O_3$ Doped Bioactive Silicate Glasses" is based on the results of investigations carried out by me in the Physics Discipline at the School of Physical and Applied Sciences,Goa University under the Supervision of Dr. Reshma Raut Dessai and the same has not been submitted elsewhere for the award of a degree or diploma by me. Further , I understand that Goa University or its authorities will not be responsible for the correctness of observations / experimental or other findings given the dissertation.

I hereby authorize the University authorities to upload this dissertation on the dissertation repository or anywhere else as the UGC regulations demand and make it available to any one as needed.

Signature:_____

Name: Vishvam U Naik

Seat no: 22P0430046

Date: 08 | 05 | 2024

Place: Goa University

i

COMPLETION CERTIFICATE

This is to certify that the dissertation report "Study of Structural Properties of $MnO_2 - Fe_2O_3$ Doped Bioactive Silicate Glasses" is a bonafide work carried out by Mr.Vishvam Umanath Naik under my supervision in partial fulfilment of the requirements for the award of the degree of M.Sc in Physics at the School of Physical and Applied Sciences,Goa University.

Signature :_____

Supervisor : Dr.Reshma Raut Dessai

Date: 08|05|2024

_____

Signature of Dean of School

Date: 08|05|2024

Place: Goa University

School Stamp

ii

PREFACE

This project report has been prepared in partial fullfilment of the requirement of subject PHY-651 Discipline specific Dissertation of the programme M.Sc.in Physics for the academic year 2023-2024. The project report entitled "Study of structural properties of $MnO_2 - Fe_2O_3$ doped bioactive Silicate glasses", focuses on Bioactive glasses which revolutionized the bio-material industries in terms of healthcare because of its ability to bind effectively with the material and the host living tissue.The study is structured into four chapters, each of which holds its own significance and relevance.

Chapter 1: This Chapter provides Introduction and overview of glasses, tracing their historical development and offering a clear definition. It also presents a concise introduction to bioactive glasses, highlighting their various applications . Moreover, it outlines the objectives of the study, specifying the goals pursued in examining the structural properties of $MnO_2 - Fe_2O_3$ doped bioactive silicate glasses.

Chapter 2: This chapter includes a brief Literature survey of different research papers relevant to the project study for comprehensive understanding of the existing body of knowledge, theories, methodologies, and findings.

Chapter 3: This chapter discusses the Experimental methods employed in the study, encompassing detailed descriptions of the preparation methods utilized for synthesizing the $MnO_2 - Fe_2O_3$ doped Bioactive silicate glasses, as well as the characterization techniques employed to analyze their structural properties.

Chapter 4: Analysis and results of the prepared samples along with conclusion and scope for future work.

ACKNOWLEDGEMENT

Contents

List of Figures

List of Tables

ABSTRACT

Bioactive glasses have been studied for their potential applications in health related issues. Bioactive materials have property to bond with the host living tissue. Many of the properties of these materials can be optimized by varying composition and processing techniques. These materials have not yet reached their actual potential in cancer therapy, but the relevant research activity in the field is significantly growing. Glasses having transition metal oxides in their composition are being widely studied for their magnetic and Bioactive nature, In the present study $MnO_2 - Fe_2O_3$ doped bioactive Silicate glasses have been synthesized by melt-quenching method , Xray diffraction of these samples revealed their amorphous nature , FTIR and Raman analysis showed bending and stretching vibrations of Si-O-Si group confirming glass formation, It was observed that as the Fe_2O_3 content in glass increases it becomes more denser.Analysis of the absorption spectra and refractive index of the glass samples indicated a rising trend with higher iron content, while a reduction in the optical band gap. In vitro studies were carried out by incubating the samples in simulated body fluid for 7, 14 and 20 days and it showed HAp layer formation on all the glass samples. This comprehensive exploration sheds light on the structural properties of $MnO_2 - Fe_2O_3$ doped bioactive silicate glasses, paving the way for potential biomedical applications.

Chapter 1

INTRODUCTION

1.1 A brief history of glass

The history of glass dates back millions of years ago, with evidence of its presence found in naturally occurring forms such as Fulgurite, Obsidian, and Moldavite. Fulgurite emerges from the fusion of sand struck by lightning, transforming it into delicate, branching glass structures.(Pasek, Block, & Pasek, 2012) Obsidian, a volcanic glass, forms when molten lava rapidly cools on the Earth's surface, resulting in sharp, black, glassy material used by ancient civilizations for its cutting properties.("The Editors of Encyclopaedia. "obsidian"", 2024) Moldavite, another intriguing natural glass, originates from the impact of meteorites on the Earth's surface, creating tektites with unique green hues and unusual properties. These natural glasses provide glimpses into humanity's early interactions with glass-like materials.

(a) (b) (c)
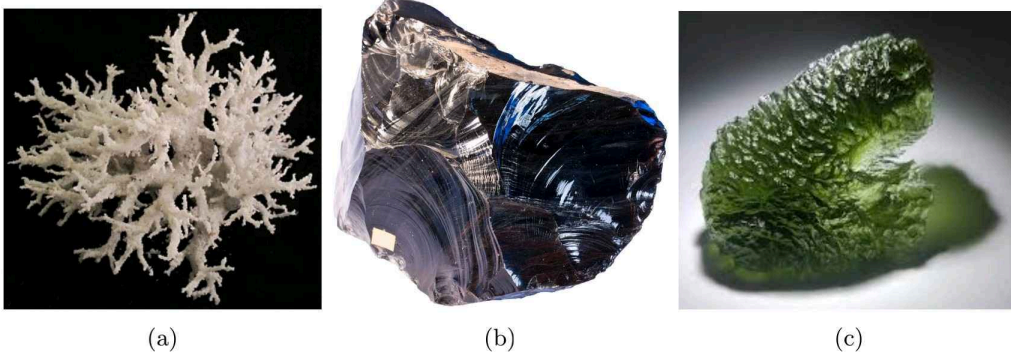
Figure 1.1: Natural glasses (a):Fulgerite,(b):Obsedian, (c):Moldavite

This showcased how our ancestors utilized natural resources for survival, as time passed people were indulged in glass making that dated back to 5000 BCE, and then there were suggestions from roman historian that Phoenician merchants had made the first glass in Syria but archaeological evidences proved that the first glass was made in eastern Mesopotamia in 3500 BCE, The introduction of the blowpipe in the 1st century BC revolutionized glass production, leading to its widespread adoption across the Roman Empire. Venice became a prominent glass-making center during the Crusades, with Murano Island becoming a hub of innovation. In the 15th century, Venetian glassblowers developed clear, nearly colorless glass, which spread to northern Europe. Lead glass was invented in England in 1674, further advancing glass-making techniques. The United States saw its first glass factory in Jamestown, Virginia, in 1608.(Chopinet, 2019) Technological advancements in the 19th and 20th centuries, such as sheet glass drawing machines and automatic bottle-blowing machines, revolutionized glass production. Innovations like safety glass and tempered glass expanded the practical applications of glass in various industries. Today, glass remains an integral part of modern life, used in construction, transportation, art, and in healthcare, with ongoing advancements continuing to drive innovation in the field.(Chopinet, 2019)

1.1.1 Defination of glass

Glass is a Non-Crystalline, metastable Solid having short range order prepared by Rapid Cooling of the Liquid (Melt).
Which exhibits glass transition temperature where the structure of glass undergoes a transition from a rigid, solid-like state to a more flexible, viscous state upon heating. In general, glass is an inorganic product of fusion that lacks the ordered and periodic arrangement of crystalline material. Since glass remains in a liquid state even when its temperature has dropped below its usual freezing point it is termed as super-cooled liquid.

1.1.2   The glass transition

Materials produced via the melt quenching method display a glass transition temperature (Tg). During the cooling process of the liquid, one of two outcomes may occur. Either the substance will crystallize at its melting point (Tm), or it will enter a supercooled state at temperatures below Tm, gradually becoming more viscous with decreasing temperature until it ultimately forms a glass.(Elliot & Download, 1985)

The crystallization event is marked by a sudden change in volume at Tm, whereas glass formation is characterized by a gradual deviation in slope. This transitional region is denoted as the glass transition temperature (Tg). Due to the continuous nature of the transition to a glassy state and the lack of a precise definition for Tg, a fictive temperature (Tf) is often employed. Tf represents the temperature at which the glass would hypothetically achieve metastable equilibrium if instantaneously cooled to that point. Despite its seeming precision, Tf is contingent upon the cooling rate of the supercooled liquid. A slower cooling rate allows for a larger supercooled region, thus resulting in a lower Tf. Therefore, the glass transition temperature of a material is influenced by its thermal history and is not an inherent property.(Elliot & Download, 1985)

1.1.3   Volume-temperature relation

Fig.1.2 shows that as the temperature of the liquid decreases from its initial state at point 'a', the volume of the substance decreases along the path 'ab'. If the cooling rate is slow and there are nuclei present in the molten material, crystallization occurs at temperature Tm, resulting in the decrease in volume along the trajectory 'bc'. Subsequently, as the crystalline material continues to cool, it contracts along the trend 'cd'.(Elliot & Download, 1985)

Conversely, when the cooling rate is considerably high, crystallization does not occur at Tf. Instead, the volume of the now supercooled liquid decreases along line 'be', which is a seamless continuation of 'ab'. At a critical temperature, Tg, the volume-temperature curve of the supercooled liquid undergoes a distinct alter-

ation in direction, aligning almost parallel to the contraction curve of the crystalline state. This temperature range, where the slope changes, defines the glass transition temperature, Tg. Between Tg and Tf, the material exists as a supercooled liquid.

Differentiating between the supercooled liquid and glass involves considering the behavior when the glass temperature is maintained constant at T, which lies below Tg. It is observed that the volume decreases gradually until it eventually reaches a point on the dashed line, a smooth continuation of the contraction curve of the supercooled liquid. This process, termed stabilization, signifies the glass's progression towards a more stable state. Above Tg, no such time-dependent changes are observed. Without crystallization, the supercooled liquid cannot attain greater stability. Over an extended period, glass can achieve increased stability at a temperature significantly below Tg.

The properties of a specific glass composition are somewhat influenced by the rate at which it undergoes cooling through the temperature range surrounding Tg. While the exact value of Tg varies depending on the cooling rate, it serves as an approximate indicator of the temperature at which the supercooled liquid solidifies upon cooling.(Elliot & Download, 1985)
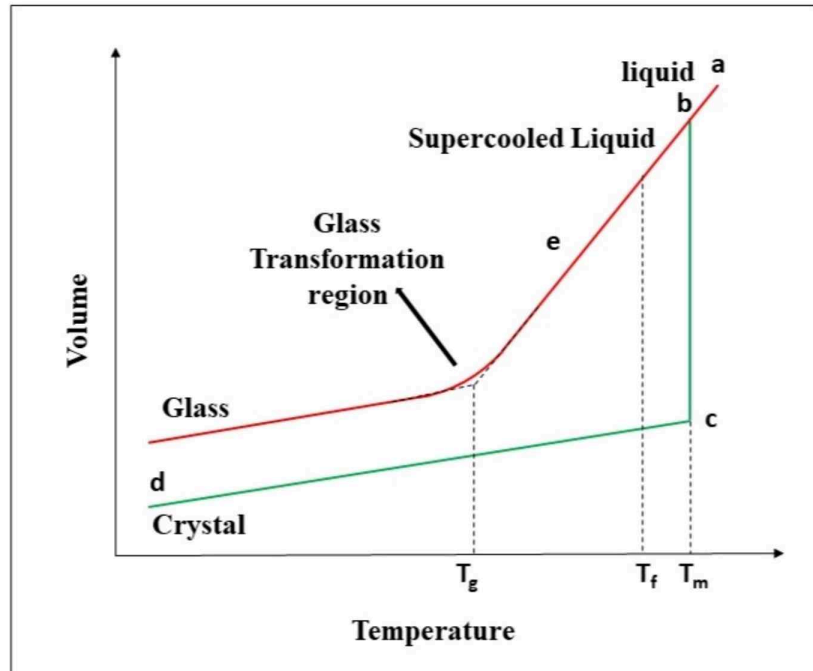
Figure 1.2: volume temperature relation

1.1.4 Structure of glass

In contrast to crystalline solids, which demonstrate a consistent atomic arrangement over long distances, glass lacks such regularity and instead presents a disordered atomic structure. This amorphous nature arises from the rapid cooling of a molten substance, which prevents the formation of a crystalline lattice. The foundational components of glass structure are network-forming atoms, typically silicon and oxygen, which bond to construct a three-dimensional network. These atoms are linked together by bridging oxygen atoms, establishing a continuous framework that imparts strength and stability to glass. Additionally, glass may incorporate network modifiers and intermediary elements, which disturb the network structure and introduce variations in its properties.(Elliot & Download, 1985)
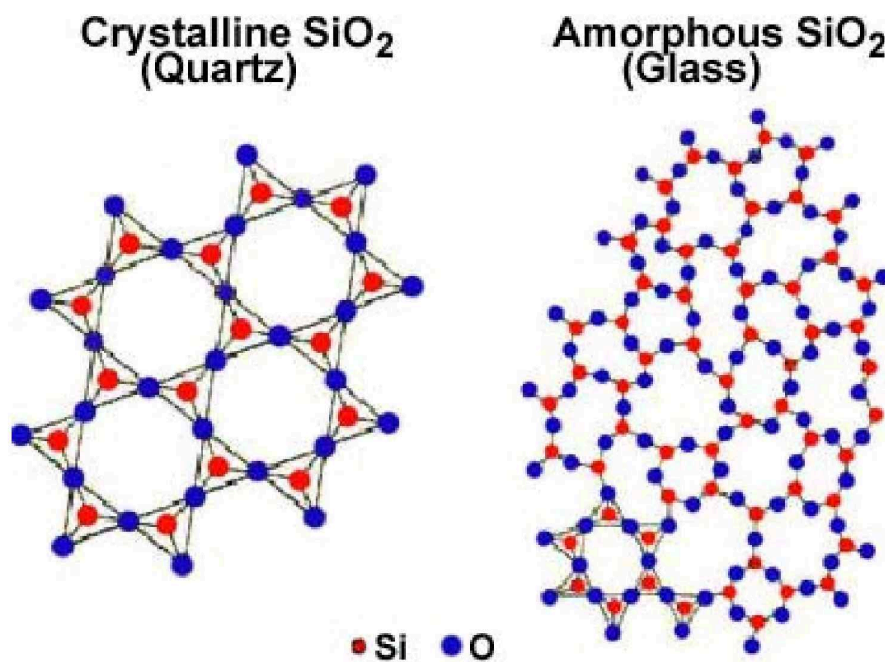
Figure 1.3: Schematic 2D representation of crystalline and amorphous compound

Glass forming ability of different oxides was first studied by the physicist John J. Zachariasen in 1932,and was called zachariasen random network theory, which is a model used to describe the structure of disordered materials, particularly glasses. The theory attempts to explain the amorphous nature of glasses, which lack the

long-range order like crystalline materials.

Zachariason proposed four rules which an oxide must obey in-order to form of glass.(Elliot & Download, 1985)

1. An oxide atom is linked to not more than two glass forming atoms.

2. The glass forming atom should have small coordination number.

3. The oxygen polyhedra share the corners with each other, not edges or faces.

4. The polyhedra are connected in a three dimensional network.

In Zachariasen's model, the atoms or molecules in a glass are arranged in a random network of interconnected polyhedra. These polyhedra are irregularly shaped and share vertices and edges, creating a three-dimensional network. This network structure provides mechanical rigidity to the glass while allowing for the lack of long-range order characteristic of an amorphous material. One of the key features of Zachariasen's random network theory is that it accounts for the observed properties of glasses, such as their isotropy (uniformity of properties in all directions) and lack of sharp melting points. The theory also explains phenomena like glass transition temperature, where a glass transitions from a supercooled liquid state to a solid-like state upon cooling. While Zachariasen's model provides valuable insights into the structure of glasses, it has limitations, particularly in its oversimplified treatment of the atomic interactions within the glass network. Modern research continues to refine our understanding of glass structure and properties, incorporating insights from both experimental techniques and computational modeling. (Elliot & Download, 1985)

1.2 Silicate Glass

Silicate glass is a type of glass primarily composed of silica (silicon dioxide, SiO2) along with various other compounds such as phosphorous pentoxide(P2O5), sodium oxide (Na2O), calcium oxide (CaO). Fig 1.4 represents, the dashed lines symbolize half-bonds extending throughout three-dimensional space. Each oxygen atom functions as a bridging oxygen, facilitating its shared presence between adjacent silicon atoms. Despite the chemical formula indicating SiO2, it is conceptually viewed as comprising silicate groups.

$$([SiO_4]^{4-})$$
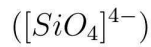
,where oxygen ions are shared among neighboring silicon ions, resulting in a charge-neutral compound. The stoichiometry equation can be represented as

$$Si + 4(\frac{1}{2}O) = Si + 2O = SiO_2$$
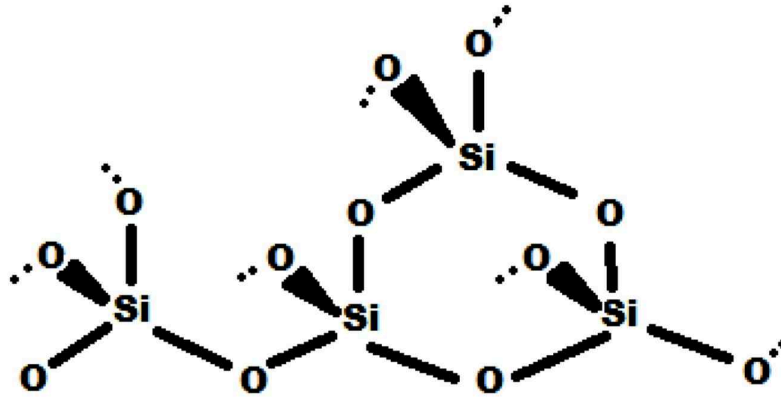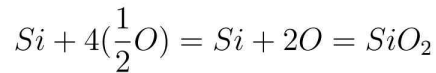
Figure 1.4: Tetrahedral arrangement of SiO_2

1.2.1 Silicon dioxide

Silicon dioxide SiO_2 is the most used network former for glass structure. It forms the foundation of most glass compositions, providing stability and strength to the material. In its pure form, silica exists as crystalline quartz, but when combined with other elements and melted at high temperatures, it transforms into an amor-

phous solid structure characteristic of glass.The silicon-oxygen (Si-O) bonds in silica are highly stable, contributing to the durability of glass. Silica's ability to undergo various modifications, such as adding dopants or modifiers, allows for the customization of glass properties to suit specific applications. Adding metal oxides to silica can alter its refractive index, making it suitable for optical applications.

1.2.2 Phosphorous pentoxide

Phosphorus pentoxide,(P_2O_5) also serves as a network former in specialized glasses, similar to silica (SiO_2) in silicate glasses.A three-dimensional network structure is formed by linkage of phosphorus atoms to the oxygen atoms. This network structure imparts mechanical strength and stability to the glass, while also influencing its optical and thermal properties.It also has applications in areas such as biomedical engineering and optical amplifiers.

1.2.3 Calcium oxide

Calcium oxide, which is obtained from limestone or dolomite, acts as a network modifier in specific glass compositions. Unlike sodium and potassium oxides, which primarily enhance the workability of glass, calcium oxide contributes to its strength and durability. It establishes stable calcium-oxygen (Ca-O) bonds within the glass network, reinforcing its structure and rendering it less vulnerable to breakage and chemical corrosion. Glass formulations incorporating calcium oxide find widespread use in architectural and automotive applications, where resilience against environmental factors is crucial. Moreover, glasses modified with calcium exhibit enhanced thermal and electrical properties, broadening their applicability in specialized sectors like electronics and telecommunications.

1.2.4 Sodium oxide

Sodium oxide (Na_2O) are widely used as network modifiers in glassmaking. By replacing some of the network-forming elements like silicon and boron, these oxides disrupt the rigid network structure, thereby lowering the glass's viscosity and melting

point. Additionally, sodium and potassium ions can act as fluxes, promoting the fusion of silica particles and reducing the energy required for glass melting. This fluxing effect is particularly advantageous in large-scale glass production, where energy efficiency and throughput are paramount considerations.

1.2.5 Manganese dioxide

Manganese dioxide,naturally occurring black-brown solid represented by the chemical formula MnO_2, serves as a decolorizing agent in glassmaking. Its stability under high temperatures is essential for glass production. Moreover, its presence influences the absorption properties, bandgap, and refractive index of the material.

1.2.6 Iron Oxide

Iron oxide, known as ferric oxide and represented by the chemical formula Fe_2O_3, is an inorganic compound abundant in nature and is widely dispersed. It plays a multifaceted role in glass formation, influencing coloration, stability, and fluxing characteristics. Additionally, due to its ferromagnetic nature, iron oxide can also modify the magnetic properties of glass.

1.3 Bioactive Glass

Bioactive glasses are non-crystalline silicate based materials renowned for their compatibility with the human body, ability to fuse with bone, and capacity to stimulate the regeneration of new bone tissue while gradually dissolving over time. This characteristic provides promise in restoring diseased or damaged bone, aiming to rejuvenate it to its original state and functionality,commonly referred to as bone regeneration.(JONES, 2008)

The pioneering discovery of bioactive glass traces back to 1969 when Larry Hench and his team at the University of Florida unveiled the first material capable of forming a robust bond with host tissue upon implantation (Hench et al., 1971). This milestone marked a pivotal moment in biomaterials research which opened doors to a new possibilities in the field of regenerative medicine.(JONES, 2008)

The initial bioactive glass composition comprised of 46.1% SiO_2, 24.4% Na_2O, 26.9% CaO, and 2.6%P_2O_5, measured in mol% also known as 45S5 Bioglass. This formulation laid the foundation for subsequent advancements and innovations in the realm of bioactive materials.(JONES, 2008)

1.3.1 Mechanism of bone bonding

The mechanism behind the bonding of bioactive glasses to bone is attributed to the creation of a carbonated hydroxyapatite (HCA) layer on the surface of the glass upon contact with bodily fluids.(JONES, 2008) This HCA layer, resembling bone mineral, facilitates the formation of a durable bond between the implant and the surrounding bone tissue. The formation of the HCA layer occurs through a rapid series of chemical reactions initiated on the implant's surface when exposed to bodily fluids (Pantano et al., 1974; Greenspan and Hench, 1976; Hench, 1998b, 1991). According to JR JONES et al.,(JONES, 2008) These reactions progress through five proposed stages, resulting in the swift release of soluble ionic species and the development of a bi-layer composed of hydrated silica and polycrystalline hydroxy carbonate apatite (HCA) on the glass surface.

1. Rapid exchange of Na^+ and Ca^{2+} with H^+ or H_3O^+ from solution,causing hydrolysis of the silica groups, which creates silanols (Si-OH),

$$Si - O - Na^+ + H^+ + OH^- \longrightarrow Si - OH^+ + Na^+_{(aq)} + OH^-$$

   Ion exchange is diffusion controlled with a $t^{\frac{1}{2}}$ dependence. The pH of the solution increases as a result of H^+ ions in the solution being replaced by cations.

2. In the initial stage, the concentration of hydroxyl ions in the solution increases, leading to the attack on the silica glass network. This results in the release of soluble silica in the form of Si(OH)4 into the solution, caused by the breaking of Si-O-Si bonds and the continuous formation of Si-OH (silanols) at the interface between the glass and the solution.

$$Si - O - Si + H_2O \longrightarrow Si - OH + OH - Si$$
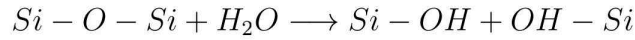
   An interface-controlled reaction with a $t^{1.0}$ dependence can be seen in the above stage.

3. : Following this, it is believed that condensation and repolymerization take place among the Si-OH groups, resulting in the formation of a silica-rich layer on the surface. This layer is characterized by a reduction in alkalis and alkali-earth cations.

4. Ca^{2+} and PO_4^{3-} groups then migrate to the surface through the silica-rich and from the surrounding fluid, forming a $CaO–P_2O_5$ rich film on top of the silica-rich layer.

5. The $CaO–P_2O_5$ film crystallises as it incorporates OH^- and CO_3^{2-} anions from solution which then form a mixed hydroxycarbonate apatite (HCA) layer.(JONES, 2008)

1.3.2 Hyperthermia treatment of cancer

The term "hyperthermia" is derived from the Greek words "hyper," meaning raising, and "therme," meaning heat. Essentially, hyperthermia involves raising the temperature of a specific part of the body above normal levels and sustaining it for a defined duration. It entails heating malignant cells to temperatures close to 43°C using either external or internal methods while minimizing damage to neighboring normal cells. Within the temperature range of 42–46°C, cell apoptosis occurs, leading to programmed cell death. At even higher temperatures, around 48°C, cell necrosis takes place, resulting in cell death. Both of these mechanisms contribute to the eradication of malignant cells while sparing nearby healthy tissue.(S. Danewalia & Singh, 2021) Hyperthermia has been a part of clinical practice for many years. Its benefits are particularly notable in scenarios where solid tumors are difficult to overcome with conventional radiotherapy and chemotherapy . Certain tumors exhibit resistance to drugs and radiation, and cannot be eliminated by standard chemotherapy and radiation therapy. In such instances, hyperthermia emerges as a more effective option.(S. Danewalia & Singh, 2021)

1.3.3 Magnetic induced hyperthermia

Magnetic hyperthermia was initially proposed based on the heat generation capabilities of iron oxide owing to hysteresis losses . When heat is produced using alternating magnetic fields, it is termed Magnetic Induction Hyperthermia (MIH). In MIH, ferrimagnetic, ferromagnetic, or superparamagnetic materials, often referred to as thermoseeds, are introduced into tumor cells. These thermoseeds react to externally applied alternating magnetic fields by generating heat through different mechanisms.(S. Danewalia & Singh, 2021)Fig.1.5 illustrates a schematic of MIH treatment. Ferri-magnetic or ferromagnetic thermoseeds exhibit magnetic hysteresis under the influence of the alternating magnetic field. The magnetic moments of these materials attempt to align with the direction of the magnetic field. However, complete reversal of magnetic moments does not occur upon reversal of the magnetic field direction. As a result, the magnetization versus applied magnetic

field graph displays a hysteresis loop. The enclosed area by this loop represents the work done during the reversal of magnetic moments with the changing magnetic field. This work is converted into thermal energy, which is then dissipated to the surrounding environment. Consequently, tumor cells are killed due to the resultant heat.(S. Danewalia & Singh, 2021)
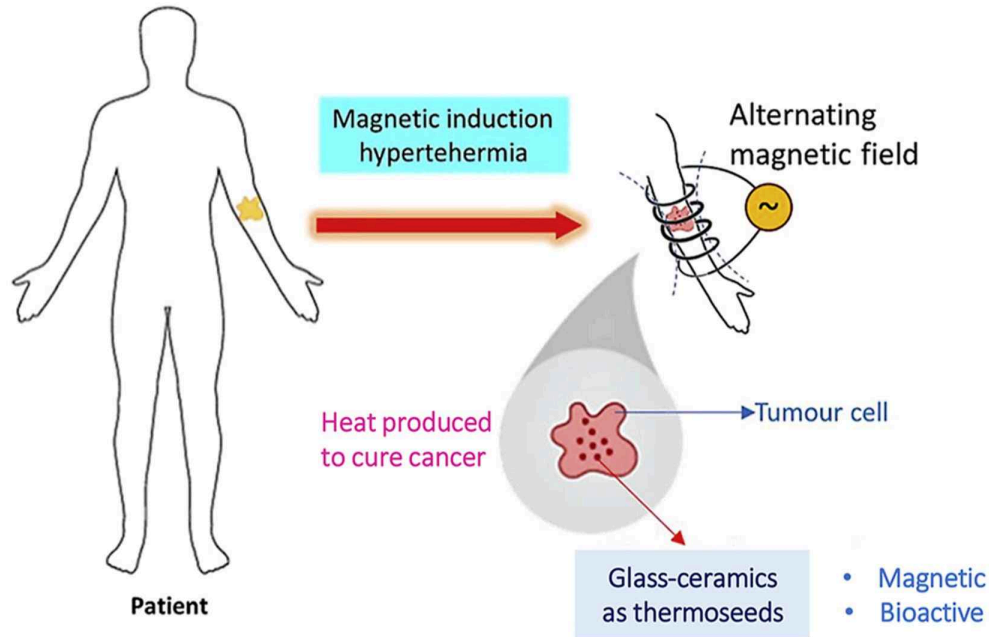
Figure 1.5: Magnetic induction hyperthermia
(S. Danewalia & Singh, 2021)

1.4 Objectives

1. To synthesize Bioactive glasses containing (MnO_2, Fe_2O_3) by melt quenching.

2. To Characterize the prepared glasses for their structural properties using XRD, FTIR, RAMAN , UV-VIS and SEM.

3. To perform In-vitro studies on the glasses to test bioactivity by immersing the material in Simulated body fluid and studying the influence of composition on bioactivity and characterize them using XRD and SEM.

Chapter 2

<u>LITERATURE REVIEW</u>

1) D. Bizari et al. "$BaO\text{--}Fe_2O_3$ containing bioactive glasses: A potential candidate for cancer hyperthermia," (Bizari, Yazdanpanah, & Moztarzadeh, 2020). In their study, they synthesized bioactive glass containing $BaO\text{--}Fe_2O_3$ using sol-gel synthesis. The physical, morphological, and magnetic properties of these glasses were investigated using X-ray diffraction (XRD), scanning electron microscopy (SEM), transmission electron microscopy (TEM) and Vibrating scanning magnetometer(VSM), Thermal properties were analyzed based on the differential thermal analysis (DTA) plot of the prepared samples. The findings revealed that the addition of $BaO\text{--}Fe_2O_3$ to the glass structure significantly influenced its magnetic behavior. Vibrating Sample Magnetometer (VSM) and calorimetric tests demonstrated that the magnetic behavior of the glasses increased with the magnetic content's augmentation. Specifically, BG1010 and BG0515 glass compositions exhibited sufficient heat generation for potential application in cancer hyperthermia treatments. Considering bioactivity, and magnetic properties, the study concluded that the BG1010 sample appeared to be the most promising candidate for use in hyperthermia treatments.

2) Rajendra Kumar Singh et al. conducted a study on "Magnetic properties of bioactive glass-ceramics containing nanocrystalline zinc ferrite" (Singh & Srinivasan, 2011). In this work the glasses/glass-ceramics containing zinc ferrite were prepared using melt-quenching method , x-ray diffraction was performed on the sample for

phase identification which revealed that as the zinc-iron oxide content increases the average crystallite size also increases from 10nm to 25nm.Room temperature magnetic hysteresis (M-H) loops of glass samples at magnetic field strength of +/-20KOe and 500 Oe using Vibrating Sample Magnetometer(VSM).They observed that magnetic field increases with increase in zinc-iron oxide concentration , Area of hysteresis loop increases with increase in Zinc-iron oxide content, as area under hysteresis loop is proportional to energy loss in form of heat.thus it was concluded that samples with higher zinc iron oxide content are capable of generating more heat thus would act as a potential candidate for hyperthermia treatment of cancer.

3)Sajjad Omidian et al. "The effect of vanadium ferrite doping on the bioactivity of mesoporous bioactive glass-ceramics".(Omidian, Haghbin Nazarpak, Bagher, & Moztarzadeh, 2022)This study involved the synthesis of mesoporous bioactive glass-ceramics modified with varying concentrations of vanadium and iron through a sol–gel approach. Subsequently, the impact of these modifications on particle morphology and the biomineralization process was assessed under simulated body fluid (SBF) conditions. Analysis of N2 adsorption isotherms indicated the presence of a mesoporous structure in the samples. Moreover, Fourier-transform infrared spectroscopy (FTIR) spectra of the samples following immersion in SBF for varying durations (7, 14, and 21 days) revealed the formation of new chemical bonds associated with the apatite phase, a finding corroborated by scanning electron microscopy (SEM) observations. X-ray diffraction (XRD) patterns of the samples post-SBF immersion demonstrated that lower levels of vanadium and iron contributed to the development of a stable and more crystalline hydroxyapatite phase.

4) Satwinder Singh Danewalia et al., "conducted a study on "Magnetic and bioactive properties of MnO_2/Fe_2O_3 modified $Na_2O - CaO - P_2O_5 - SiO_2$ glasses and nanocrystalline glass-ceramics."(S. S. Danewalia & Singh, 2016) Glass and in-situ nanocrystalline glass-ceramics composed of $45SiO_2$-$25CaO$-$10Na_2O$-$5P_2O_5$-xFe_2O_3-(15-x)MnO_2 were fabricated via the melt-quenching technique, and their

magnetic and in-vitro bioactive properties were examined. The presence of a ferrimagnetic character was noted in the in-situ nanocrystalline glass-ceramics with higher Fe2O3 content. Saturation magnetization and coercivity demonstrated an increase with the addition of Fe_2O_3. Upon immersion in simulated body fluid (SBF), both powdered and bulk glasses and glass-ceramics underwent analysis using various characterization techniques. The inclusion of MnO_2 led to enhanced leaching of Na+ ions from the glasses and facilitated the attraction of Ca2+ cations from the SBF compared to Fe_2O_3-containing nanocrystalline glass-ceramics. Additionally, MnO_2 promoted the formation of a hydroxyl apatite (HAp) layer. Confirmation of HAp formation on the surface of all glasses and glass-ceramics after SBF immersion was provided by Fourier Transform Infrared (FTIR) spectra, X-ray diffraction, and scanning electron micrographs (SEM). Urbach energy measurements further indicated structural modifications on the surfaces of the glass and glass-ceramics post-SBF immersion.

5)M. Dziadek et al. conducted a comprehensive investigation on "Gel-derived SiO_2–CaO–P_2O_5 bioactive glasses and glass-ceramics with modifications through SrO addition"(Dziadek et al., 2016). Their study delved into the impact of SrO substitution for CaO on the structure (assessed via X-ray diffraction (XRD) and Fourier-transform infrared spectroscopy (FTIR)) and bioactivity (evaluated through simulated body fluid (SBF) tests) in sol-gel glasses featuring two distinct chemical compositions (silica-rich and calcium-rich glass samples). The alterations in material properties following heat treatment at 700°C and 1300°C were thoroughly explored.The findings revealed that the effect of strontium substitution on structure, bioactivity, and crystallization post-treatment at both temperatures significantly relied on the CaO/SiO_2 molar ratio. The augmentation of strontium concentration in silica-rich materials post-sintering resulted in the emergence of calcium strontium phosphate in lieu of calcium phosphate. The assessment of bioactivity suggested that Sr substitution for Ca delayed the formation of calcium phosphate solely in the case of silica-rich glasses treated at 700°C. Conversely, calcium-rich glasses ex-

hibited high bioactivity post both temperature treatments, with the crystal size of hydroxyapatite decreasing with increasing Sr content. Notably, high-temperature treatment of high-silica glasses hindered their bioactivity.

6)Francesco Baino et al., "Fe-Doped Sol-Gel Glasses and Glass-Ceramics for Magnetic Hyperthermia"(Baino et al., 2018), in this study they worked on synthesis and characterization of novel Fe-containing sol-gel materials obtained by modifying the composition of a binary SiO_2- CaO parent glass with the addition of Fe2O3. The effect of different processing conditions (calcination in air vs. argon flowing) on the formation of magnetic crystalline phases was investigated. The produced materials were analyzed from thermal (hot-stage microscopy, differential thermal analysis, and differential thermal calorimetry) and microstructural (X-ray diffraction) viewpoints to assess both the behavior upon heating and the development of crystalline phases. N2 adsorption–desorption measurements allowed determining that these materials have high surface area (40–120 m2/g) and mesoporous texture with mesopore size in the range of 18 to 30 nm. magnetic properties were studied using VSM and it was found that magnetic properties can actually be tailored by controlling the Fe content and the environmental conditions (oxidant vs. inert atmosphere) during calcination. The glasses and glass-ceramics developed in this work show promise for applications in bone tissue healing which require the use of biocompatible magnetic implants for hyperthermia for bone cancer treatment.

Chapter 3

EXPERIMENTAL METHODS

3.1 Glass preparation methods

Glass, being an amorphous solid, is formed by rapid cooling of a molten material so that its atoms cannot arrange themselves into a regular crystalline structure. This rapid cooling introduces excess free energy into the system, making the amorphous phase less thermodynamically stable than its crystalline counterpart. The faster the rate of cooling, the further the resulting glass lies from thermodynamic equilibrium. Different methods are used for making amorphous glassy materials in various forms like bulk,sheet,powder,thin films etc.

Following are the common techniques used to prepare amorphous glassy material:

- Chemical Vapour deposition

- Sol-gel technique

- Melt-Quenching method

In present study we are using melt-quenching method

3.1.1 Chemical Vapour deposition

Chemical vapour deposition (CVD) encompasses a range of techniques where a solid material is grown by reacting gaseous source substances, resulting in a gas effluent carrying the product. Variants of this process exist, differing in pressure, reactant

types, and activation methods. CVD can operate in atomic layer deposition (ALD) mode, where individual atomic layers are sequentially produced.Compared to physical vapor deposition, CVD offers several advantages. Selectivity in deposition is more achievable, allowing material to be deposited only in specific regions of the substrate, rather than uniformly covering it. CVD can handle larger substrate batches compared to evaporation and is less sensitive to precise process conditions.("Chemical Vapor Deposition", 2008)

3.1.2 Sol-gel technique

This method has its usefulness for those systems which give rise to very viscous melts near melting points or have extremely high melting points posing technical problems in melt quenching. There are two routes to produce an amorphous materials via gel either using aqueous or organic materials as the starting component.

1. **Aqueous process**

   Destabilization of sol (mostly of silica) with other components being added in the form of appropriate aqueous solution. Silica together with any desired network modifiers are formed into an aqueous sol,It is then converted into a rigid gel by progressive polymerization and formation of branched network, which is then transformed into dense glass by sintering or fusion.

2. **Organic metallic process**

   Alkoxysilicane with any desired network modifiers in the form of metal alkoxides or salts are formed into a sol which is then polymerized and gelled by partial hydrolysis and heat treated to remove any volatiles to produce dense glass

In both methods, a multicomponent gel (homogeneous and non crystalline) is heated to remove volatile components and cause an initial densification, completed by a final process of sintering or fusion to produce the amorphous solid. (Elliot & Download, 1985)

3.1.3 Melt-quenching method

Melt-quenching method is the most used primary preparation technique used in glass industries as well as research field. In this method glass is prepared by rapid cooling of the molten sample which shows glass transition temperature. In this method the sample is prepared by weighing the calculated amount and then crushed and mixed with the help of agate mortar to obtain a fine talcum like texture which is then heated at high temperature to melt the molten melt and than air quenched quickly on a steel plate preventing crystallization to obtain a dense glass. The prerequisite for glass formation is faster cooling to prevent crystallization. Being thermodynamically more stable crystal growth will always dominate over the amorphous phase formation if allowed. Using this technique we can prepare large number of silicate, borate, phosphate, oxide or non oxide composition of glasses. The doping or codoping of different types of active ions is quiet easy using this method. The rate of cooling varies enormously from material to material. When glass is made, the material is quickly cooled from a super-cooled liquid, an intermediate state between liquid and glass. To become an amorphous solid, the material is cooled, below a critical temperature called the glass transition temperature. The newly formed amorphous structure is not as organized as a crystal, but it is more organized than a liquid.(Elliot & Download, 1985)

3.2 Preparation of Silicate Glasses

The desired Sodium silicate glass was prepared by using Silicon dioxide(SiO_2) as a network former along with phosphorous pentoxide(P_2O_5), calcium Oxide(CaO) and Sodium Oxide(Na_2O) acted as network modifier while manganese dioxide(MnO_2) and Iron oxide(Fe_2O_3) were the intermediates used for doping to enhance different properties like magnetic properties also to study its effect on the composition of glasses.The composition of glasses is shown in Table 3.1

Table 3.1: Composition of as prepared glasses

Sample label	SiO$_2$	CaO	Na$_2$O	P$_2$O$_5$	MnO$_2$	Fe$_2$O$_3$
BG00	45	24	24	7	0	0
BG11	45	23	23	7	1	1
BG22	45	22	22	7	2	2
BG33	45	21	21	7	3	3
BG1010	45	14	14	7	10	10

Glasses with above composition was prepared by melt-quenching method ,the raw materials used were sodium carbonate(Na_2CO_3), calcium Carbonate ($CaCO_3$) and Ammonium dihydrogen phosphate ($[NH_4]H_2PO_4$).Other chemicals were taken in their Original oxide form. With respect to the raw materials and compounds sto-ichmetric calculation were made for each glass composition of 1g and 5g. The calculation for glass batch BG00 is shown in table 3.2 , batch calculation for BG11,BG22, BG33, BG1010 should follow the same.

Table 3.2: Composition of BG00 Sample

Compound	Mol %	MW of Compound	MW of Raw material	Mass (g)	
SiO$_2$	45	60.0843	60.0843	0.45	2.25
Na$_2$O	24	61.9794	105.99	0.41	2.05
CaO	24	56.072	100.09	0.43	2.14
P$_2$O$_5$	7	141.94	230.06	0.11	0.56
MnO$_2$	0	86.94	86.94	0	0
Fe$_2$O$_3$	0	159.6882	159.6882	0	0

The bioactive glass with composition as shown in Table 3.2 were synthesized by melt quenching technique. All the chemicals used in the preparation were of analytical grade 99% pure. First trial for glass preparation was carried out for 1gm sample in alumina boat. After glass formation is confirmed, 5 gm glass composition was crushed in pestle and mortar and placed in furnace and temperature was held at 850 °C for decomposition of calcium carbonate. The temperature of furnace was increased to 1400 °C according to the schedule. The compound melted and a bubble free viscous liquid was formed and then rapidly air quenched into a steel plate using

pair of tongs. The glass beads of different sizes and shapes formed were placed in preheated furnace at temperature 360 °C for 1 hour for annealing. A typical heating schedule for 1 such sample is shown in Fig 3.1, the glass samples are shown in Fig 3.3.
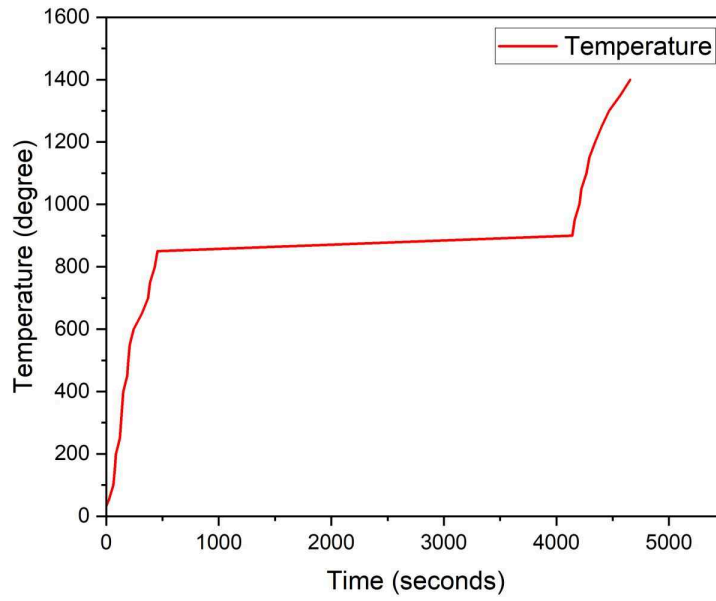

Figure 3.1: Heating Schedule of BG00

Figure 3.2: Air quenching of glass

Figure 3.3: Glass samples

3.3 Preparation of Simulated body fluid (SBF)

The SBF solution was prepared by dissolving chemicals $NaCl, NaHCO_3, KCl,$ $K_2HPO_4.3H_2O, MgCl_2.6H_2O, CaCl_2, Na_2SO_4$ in de-ionized water. This dissolved mixture was kept on a magnetic stirrer which had a programmable heat supply and was kept at 37°C . The pH of the solution was maintained at 7.4 by titration using prepared 1N-HCl while stirring. Once the pH became 7.4 the solution was transferred to a 200 ml volumetric flask,the total volume of the solution was then adjusted to 200 ml by adding the de-ionized water and shaking the flask for complete mixing. The flask was then kept for refrigeration at 5-10 °C.(Kokubo & Takadama, 2007) The glass powder was soaked in synthesized Simulated body fluid (SBF) solution in a petridish for time period of 7,14 and 20 days and placed in an Incubator at temperature 37°C which is the human body temperature. The samples were immersed completely with SBF solution. These samples taken out at each intervals for further characterization.

Figure 3.4: Immersed samples in SBF

Figure 3.5: Samples in Incubator

3.4   Density of glass

Density of a glass was measured by Archemedes principle by first obtaining weight of glasses in air and then in water using set up shown in Fig 3.6. Density of glass refers to the measure of how much mass is contained within a given volume of glass and it is expressed as g/cm^3 or kg/m^3. Density calculated using formula:

$$\rho_{glass} = \frac{W_{air}}{W_{air} - W_{water}} \times \rho_{water}$$

Figure 3.6: Set up for density measurement

3.5 X-ray Diffraction

Powder X-ray diffraction (XRD) is a common characterization technique to identify phase of the materials. Analysis of a sample by powder XRD provides important information that is complementary to various microscopic and spectroscopic methods, such as phase identification, sample purity, crystallite size, and, in some cases, morphology. As a bulk technique, the information it provides can be correlated with microscopy data to test if microscopic observations on a small number of particles are representative of the majority of the sample.(Holder & Schaak, 2019) X-ray diffractometer consist of : an X-ray tube, a sample holder, and an X-ray detector. X-rays are generated in a cathode ray tube by heating a filament to produce electrons, accelerating the electrons toward a target by applying high voltage, and bombarding the target material with electrons.

3.5.1 Principle of X-ray Diffraction

When x-rays are incident on the atomic planes of the sample, they are diffracted by the electrons,If the sample is crystalline and are arranged in a regular structure it results in maxima and minima in the diffracted intensity. The diffraction pattern helps to distinguish between amorphous and crystalline material. In crystalline materials we observe a sharp peaks as their periodicity in lattice plans gives rise to constructive and destructive pattern. Whereas in amorphous material we get a broad maxima or a statistical average.

The condition for diffraction was first formulated by W.L.Bragg using a simple model. Bragg assumed that the monochromatic Xrays incident on the crystal are reflected from successive parallel atomic planes in the crystal where the angle of incidence is equal to angle of reflection, when the reflection from the parallel atomic planes interfere constructively , strong intensities known as Braggs peaks are obtained in the diffraction pattern when the maxima follow Bragg's condition.
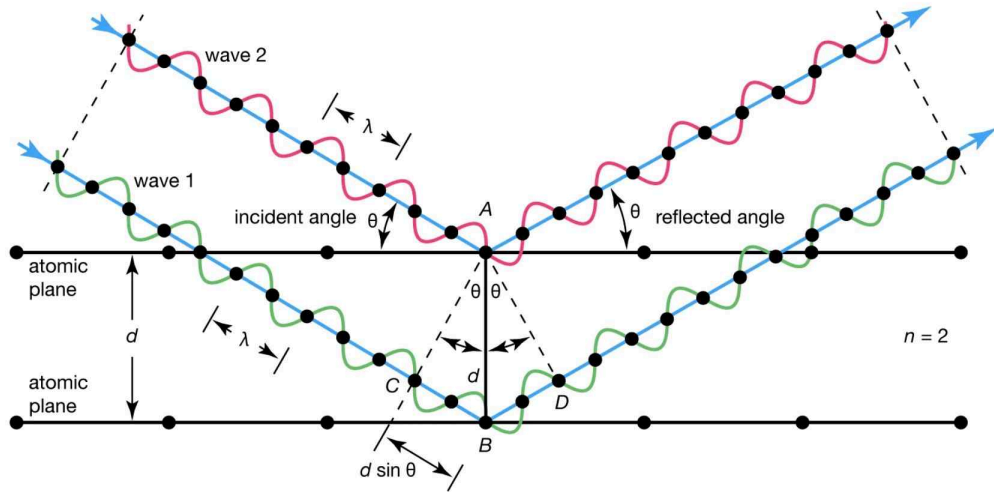
$$n\lambda = 2dsin\theta$$

where

n=integer

λ=characteristic wavelength of the x-rays impinging on the sample

d=interplanar spacing between rows of atoms

θ=angle of the x-ray beam with respect to these planes.

Figure 3.7: Bragg's Condition

The Bragg law is used in determining the wavelengths of radiation and assessing the lattice spacing's within crystals. To gauge a specific wavelength, both the radiation beam and the detector are positioned at an initial angle θ. This angle is adjusted until a notable signal is detected. The resulting Bragg angle provides a direct determination of the wavelength according to the Bragg law. This method is fundamental in accurately measuring the energy of X-rays and low-energy gamma rays. Moreover, Bragg reflection is commonly employed to ascertain the energies of neutrons, which exhibit wave-like properties according to quantum theory (of Encyclopaedia Britannica, 2023)

3.5.2 Experimental setup for x-ray diffraction

The Rigaku Xray Diffractometer is used in the experiment as shown in Figure (3.8). For x-ray diffraction experiment the glass samples were crushed to obtain powder which was than clamped to instrument by filling the XRD glass slide.The x-rays

generated from the instrument were made to incident on the sample for 2θ of 10 to 80 °C , In this experiment the incident xray beam passes through the monochromator and is collected by the detector.

Here X-ray source is fixed but the sample and the detector move together producing corresponding intensity for different angle. The electronic counter present in the instrument converts the Xrays into pulses of electronic current which is directly proportional to the intensity of the diffracted x-ray beam entering the detector slit. The diffraction pattern were observed for a set time at 5 degrees per minute within the scattering angle 2θ.

Figure 3.8: Rigaku Xray Diffractometer

3.6 Fourier Transform Infrared Spectroscopy

Fourier transform infrared (FTIR) spectroscopy, is a technique used to obtain spectrum of absorption or emission of solid or liquid. Infrared absorption spectra can provide valuable information about the arrangement of atoms, nature of chemical bonds. Within the mid-infrared region, vibrations radiate from numerous environmentally significant molecules, including organic acids, soil organic matter, mineral phases, and oxyanions. All molecules are made up of atoms which are linked by chemical bonds. Upon interaction with atoms, a portion of the incident radiation is absorbed at a particular wavelength. The molecule will absorb certain frequencies as the energy is consumed in stretching or bending different bonds.The multiplicity of vibrations occurring simultaneously produces a highly complex absorption spectrum, which is uniquely characteristic of functional groups comprising the molecule. FTIR spectroscopy offers both quantitative analytical capabilities and insights into bonding mechanisms within solids. By directly correlating molecular vibrations with molecule symmetry, it becomes feasible to precisely determine how molecules bond on surfaces or function within solid phases based on their infrared spectra.(Daéid, 2005)

3.6.1 Principle of Infrared Spectroscopy

Infrared spectroscopy operates based on the principle that all molecules exhibit vibrational motion and have the capacity to absorb energy within the infrared spectrum. Most vibrational absorption bands fall within the wavelength range of approximately 2.5 to $25\mu m$ (4000-400 cm^{-1}) . As electromagnetic radiation traverses a sample (whether it be solid, liquid, or gas), certain frequencies of the radiation are absorbed by the molecules, inducing molecular vibrations. These absorbed frequencies are distinctive for each molecule, providing a unique substance fingerprint. FTIR spectroscopy involves transmitting IR radiation through the sample, resulting in an absorption spectrum that reveals molecular information.

3.6.2 Instrumentation of FTIR Spectroscopy

At the core of every FTIR instrument lies an optical apparatus known as an interferometer. Michelson interferometer is the most widely used interfereometer. Typically, an infrared source, often a heated ceramic (approximately 1200°C), is employed. Light emitted from the source is collected and made parallel by a collimating mirror. A beamsplitter composed of KBr transmits roughly half of the incident light while reflecting the other half. A portion of the transmitted light travels to a stationary mirror, while the remaining reaches a mirror in motion . The light beams are then reflected back to the beamsplitter by the two mirrors, where they are recombined into a singular beam. This consolidated beam interacts with the sample (such as exhaust gas) within a gas cell before reaching the detector. To achieve an extended optical path length while minimizing cell volume, a multi-reflection cell is employed.(Giechaskiel & Clairotte, 2021)

The signal exiting the interferometer is a consequence of one beam traveling a fixed path length while the other undergoes continuous variation due to the movement of its mirror. This interaction between the two beams results in an interferogram, representing the intensity of light plotted against the optical path difference. These interferograms are then subjected to Fourier transformation to generate a spectrum, depicting intensity versus frequency or wavenumber.

For IR sample preparation KBr powder should be finely ground using a pestle and mortar until a very fine mixture was achieved,ensuring crystallites were not visible. FTIR spectra of the samples were taken at room temperature on Shimadzu FTIR spectrophotometer. The glass powder and KBr were mixed in the ration of 1:2 and pelletized using a hydraulic press. The spectrum of each sample was normalized to the reference spectrum of KBr.

Figure 3.9: FTIR Spectrophotometer

3.7 Raman Spectroscopy

Raman spectroscopy is a versatile method of analysis and has wide range of applications in forensic samples. It resolves most of limitations of other spectroscopic techniques. It can be used for both qualitative as well as quantitative purpose. Qualitative analysis can be performed by measuring the frequency of scattered radiations while quantitative analysis can be performed by measuring the intensity of scattered radiation.(Bumbrah & Sharma, 2016)

3.7.1 Principle and Instrumentation

Raman spectroscopy utilizes a scattering method grounded in the Raman Effect, where the frequency of a portion of scattered radiation differs from the frequency of the incoming monochromatic radiation. This technique relies on the inelastic scattering of incident radiation as it interacts with vibrating molecules, enabling the probing of molecular vibrations. A sample is illuminated with a monochromatic laser beam, leading to the generation of scattered light with a frequency distinct from that of the incident light, constituting inelastic scattering and forming a Raman spectrum.

This spectrum results from the inelastic collisions between the incident monochromatic radiation and the sample's molecules. While most scattered radiation exhibits the same frequency as the incident radiation, known as Rayleigh scattering, a small fraction displays a different frequency, known as Raman scattering. Stokes lines ap-

pear in the Raman spectrum when the incident radiation's frequency exceeds that of the scattered radiation, whereas anti-Stokes lines emerge when the incident radiation's frequency is lower. Typically, scattered radiation is measured perpendicular to the incident radiation. (Bumbrah & Sharma, 2016)

In Raman spectroscopy, the Stokes shifted Raman bands are characterized by transitions from lower to higher energy vibrational levels. Consequently, these Stokes bands tend to be more pronounced compared to anti-Stokes bands, making them the focus of conventional Raman spectroscopy. Anti-Stokes bands, on the other hand, are typically examined in the presence of fluorescing samples since fluorescence can interfere with the detection of Stokes bands.

The magnitude of Raman shifts remains independent of the wavelength of the incident radiation, although Raman scattering itself is influenced by the wavelength of the incident radiation. An essential prerequisite for obtaining a Raman spectrum from a sample is a change in polarizability during molecular vibration. Due to its low Raman scattering, water serves as an ideal solvent for dissolving samples, while glass is commonly used for optical components like mirrors, lenses, and sample cells in Raman spectrophotometers.

A Raman spectrum is typically represented as intensity versus wavelength shift. While Raman spectra can be recorded across a broad range, the Raman active normal modes of vibration for organic molecules typically occur within the range of $4000–400$ cm^-1. The specific wavenumber region covered by a Raman spectrum depends on the design of the spectrophotometer and its optical components, with typical spectra spanning between $400–5000 cm^-1$ and $4000–3800 cm^-1$.

Compared to their infrared (IR) counterparts, Raman spectra are notably simpler due to the rarity of normal Raman overtones, combination, and difference bands. Raman spectrophotometers can be categorized as dispersive or non-dispersive. Dispersive Raman spectrophotometers utilize prisms or gratings, whereas non-dispersive ones employ interferometers like the Michelson interferometer in Fourier Transform Raman spectrophotometers.

Understanding Raman spectra of compounds in solid-state requires grasping con-

cepts and mathematical treatments beyond those in molecular spectroscopy. The spectra of crystalline and amorphous solids of the same composition differ due to the presence or absence of spatial order and long-range translational symmetry, respectively. Amorphous solids can be envisioned as collections of formula units with varying bond angles and lengths influenced by chemical bond interactions with nearest neighbors, lacking spatial arrangement order. Consequently, the absence of such order precludes the observation of narrow bands typical in molecular spectroscopy. Instead, the distribution of formula units with diverse bond angles and lengths generates a range of vibrational energy states, analogous to the distribution of vibrational energy states in liquid water owing to hydrogen bonding.

Figure 3.10: Raman Spectrometer

3.8   UV-VISIBLE Spectroscopy

UV-VIS spectroscopy is the oldest analytical technique that can be defined as the spectrophotometric technique which is used to measure the intensity of light in UV (200–400 nm) and VIS (400–800 nm) regions as a function of wavelength. UV-VIS spectroscopy relies on the absorption of light at specific wavelengths by the analyte, with the absorbed radiation being quantified. This interaction between UV-VIS electromagnetic radiation and the analyte generates a spectrum, which serves as the foundation for analyzing various substances including organic, inorganic, biochemical, and pharmaceutical compounds. In this spectroscopy technique, absorption occurs at electronic energy levels of molecules, making it commonly referred to as electronic spectroscopy.UV-VIS spectroscopy operates by detecting the absorption of light, where the absorbed light is directly proportional to the quantity of analyte in a sample solution. As the concentration of analyte increases, light absorption rises linearly, while light transmission decreases exponentially. In the UV-VIS region, radiation absorption relies on the electronic configuration of the absorbing species, such as atoms, molecules, ions, or complexes.(Akash & Rehman, 2020)

3.8.1   Instrumentation of UV-VIS spectroscopy

UV-VIS spectroscopy instrument contains a lamp producing light of wavelength 200-800 nm out of which 200-400 nm wavelength is of UV light and 400-800nm wavelength is of visible light , this light than falls on a monochromater made up of two slits and one prism ,the first slit is used to focus the light parallel onto the prism which is than scattered into light of different wavelengths by prism after that specific wavelength of light is passed from second slit, this light is than converted into two different light rays of equal intensity , first ray of light fall on reference cell having buffer solution and the intensity with which the first ray falls on the reference cell same intensity of light we get back after its reflected from the cell than the second ray falls on the cell containing sample such as protein which absorbs light and the absorption depends on the factors like electronic transition,concentration and path length of the cell which is also shown by Beer-Lamberts law.$A \propto CL$ According

to Beer if the concentration is more absorption increases and from lamberts thoery if path length is more than absorption also will be more, thus light reflected from sample cell will have less intensity and thus there is net change in the intensity of the two rays entering the detector resulting in the transmittance which is than converted to absorbance and we get a graph of absorbance versus wavelength,this graph is use to interpret for maximum absorbance peak , Bandgap , refractive index etc.
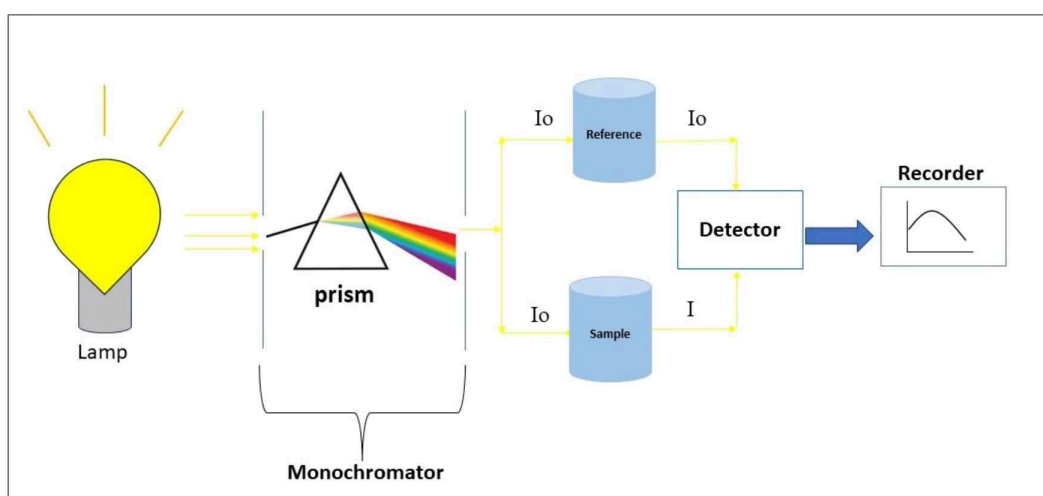

Figure 3.11: Schematic diagram of measurement of absorption spectrum of a sample.
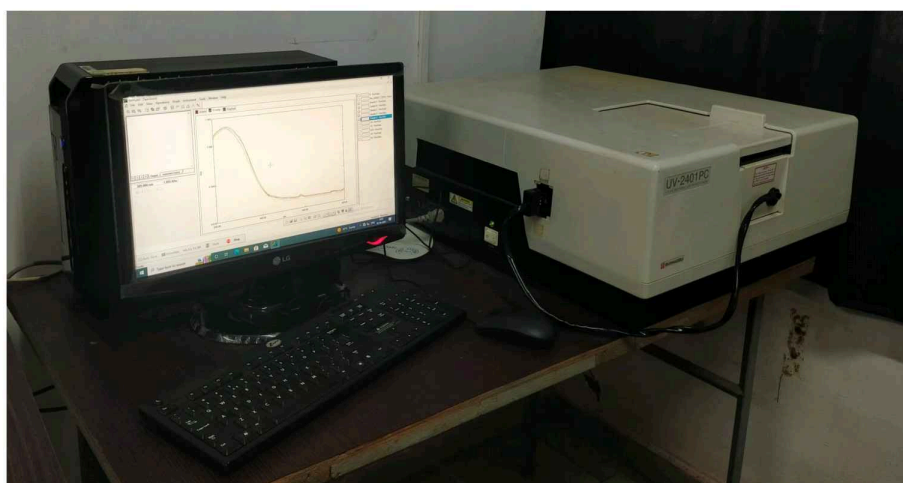
Figure 3.12: UV-VIS Spectrometer

3.9 Scanning Electron Microscopy

The scanning electron microscope (SEM) is used for examining and analyzing microstructure morphology and chemical composition characteristics. Understanding the fundamentals of electron microscopy necessitates a grasp of basic principles in light optics. The human eye can discern objects subtending about 1/60° visual angle, which translates to a resolution of approximately 0.1 mm (at an optimal viewing distance of 25 cm). Optical microscopy extends the limit of resolution to about 2,000 Å by magnifying the visual angle through optical lenses. Optical microscopy has played, and continues to play, a pivotal role in scientific research. Since the discovery in the 1890s that electrons can be deflected by magnetic fields in various experiments, electron microscopy has evolved, replacing the light source with a high-energy electron beam.(Zhou, Apkarian, Wang, & Joy, 2007)

3.9.1 Instrumentation of SEM

1. At first stage there are electron beams boasting high Electron beams ranging from 100 to 30,000 electron volts which are employed for analysis, emitted from a thermal source.

2. The electron beam initially yields a broad spot, unsuitable for sharp imaging. SEM fixes this by utilizing lenses to compress and focus the electron beam onto the specimen. Most SEMs achieve spot sizes below 10 nm, allowing electrons to interact with the specimen's surface to a depth of 1 µm, generating signals for image formation.

3. Through precise control of scan coils, the electron beam traverses the specimen's surface, creating a raster like pattern. This process, gives desired magnification. Modern SEMs automatically regulate working distance, the gap between the final lens and specimen surface, to optimize magnification.

4. Electron detectors helps in capturing emitted signals from the sample surface which is crucial for image generation. Without detectors, signals from electron-surface interactions is not understandable. SEM utilizes both secondary elec-

trons (SE) and backscattered electrons (BSE) for imaging. By manipulating the collector screen voltage, SE and BSE can be selectively collected. A Scintillator detector accommodates both SE and BSE detection.

5. Signals captured are displayed on a viewing screen, with operators adjusting brightness and intensity for clarity. High-magnification imaging, beyond 10,000x, may be necessary for detailed examination.

6. The electron voltage mode influences image resolution. Low accelerating voltages (¡5 kV) produce surface-rich images, while higher voltages (15-30 kV) penetrate deeper, revealing internal sample details.

7. SEM produces partly three-dimensional images, highlighting sample topography in terms of shape, size, and surface texture. This visualization depends on the abundance of SE and BSE, influenced by the sample's surface inclination angle. An inclination angle exceeding 50° up to 70° maximizes BSE and SE signals, enhancing topographic contrast.(Mohammed & Abdullah, 2019)
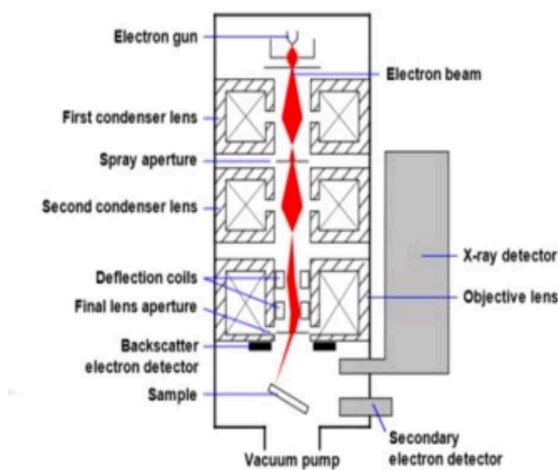
Figure 3.13: Schematic of (SEM)
(Australian Microscopy and Microanalysis
Research Facility, accessed online on 3-5-2018)

Figure 3.14: Scanning Electron Microscope

Chapter 4

ANALYSIS AND CONCLUSION

4.1 Physical Properties

Physical properties includes Density and Molar Volume , For density calculation we used the archimedes principle.The apparent densities and Molar Volume (Vm) of the prepared glasses are shown in Table 4.1 , The density of glasses is a cumulative characteristic, influenced by the original components within the composition , It was observed that as the Fe_2O_3 content is increased the glass density increases, Molar volume is the volume occupied by one mole of glass. Molar volume is calculated using formula:

$$Vm = M/\rho_{sample}$$

Table 4.1: Physical Parameters of as-prepared glasses

Sample	W	Volume (V)	Density	M(g/mol)	Vm
BG00	0.618	0.231	2.67 ± 0.15	92.60	34.59
BG11	0.494	0.182	2.71 ± 0.19	93.00	34.30
BG22	0.453	0.164	2.76 ± 0.06	93.41	33.77
BG33	5.617	0.202	2.77 ± 0.05	93.81	33.87
BG1010	0.700	0.247	2.84 ± 0.01	96.65	34.04

4.2 X-ray Diffraction

X-ray diffraction pattern of all glass samples were analyzed using Rigaku Diffractometer with incident CuKα,radiation having wavelength 1.5481A°. The data were collected in an angular range between 10 to 80 ° at the rate $5°min^{-1}$. The XRD patterns for all glasses is shown in Fig 4.1, The XRD patterns of this glasses does not have any characteristic sharp peaks instead it showed up a broad hump between 30-35° confirming the amorphous nature of glass.
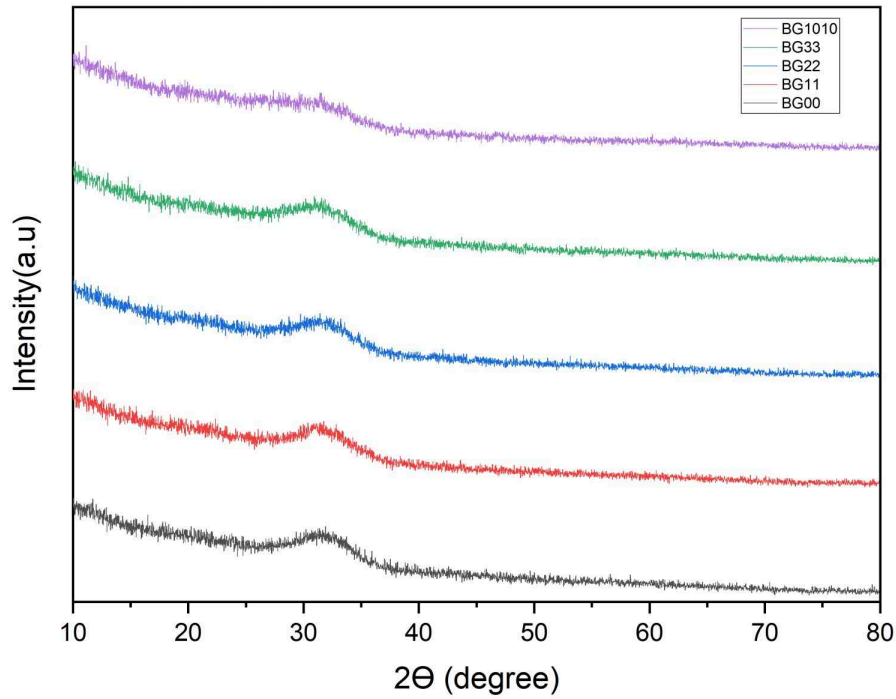
Figure 4.1: XRD patterns of the as-prepared samples.

4.3 FTIR Spectroscopy

The Infrared spectra of all the glasses have been recorded at room temperature on the Fourier transform infrared spectroscope in the frequency range 400 to 4000 cm^{-1}. FTIR spectra of the glasses have shown in Figure 4.2, It exhibits major IR bands at 460 cm^{-1}, 560 cm^{-1}, 711 cm^{-1}, and 1014 cm^{-1}. The primary features of the tetrahedral SiO$_4$ silicate lattice typically in the spectral range of 450 to 500 cm^{-1}(Omidian et al., 2022) The absorption band at around 460 cm^{-1} were related to Si-O-Si bending vibration mode and symmetric stretching of the Si-O-Si band, respectively.(Bizari et al., 2020) The metal-oxygen (Mtetra-O) vibrational mode in the range 500 - 600 cm^{-1} is evidence of the formation of a spinel phase in this material.(Omidian et al., 2022) Metal oxide bonding like (Mn-O-Mn) stretching at 711 cm^{-1} confirms the presence of manganese dioxide (MnO$_2$). The absorption band located at 1000 - 1200 cm^{-1} confirms Si-O-Si asymmetric stretching in the SiO$_4$ Group.(Hastuti, Subhan, Amonpattaratkit, Zainuri, & Suasmoro, 2021)
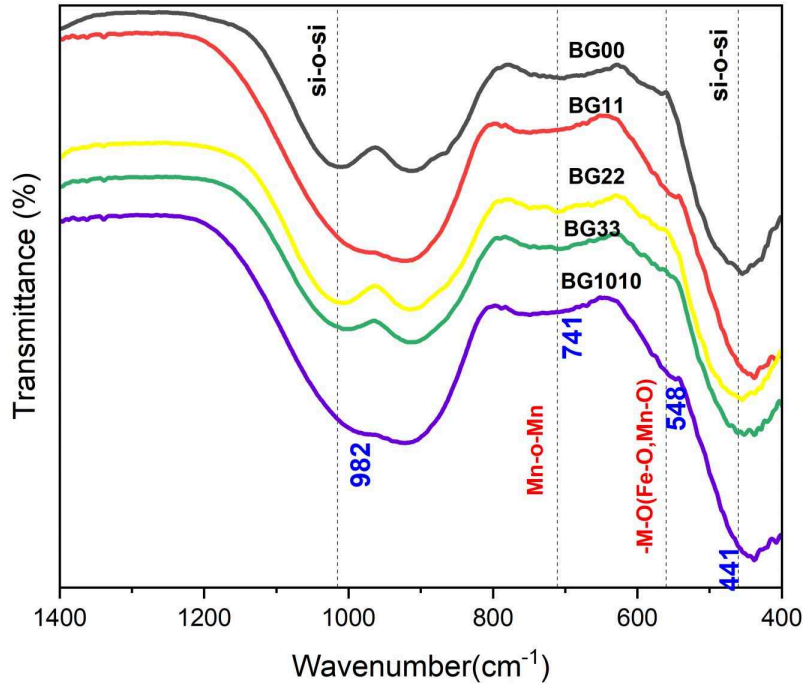
Figure 4.2: FTIR spectra of the as-prepared samples

Table 4.2: FTIR data of as-prepared samples

Sr. No	Samples					Assignment
	BG00	BG11	BG22	BG33	BG1010	
	Wavenumber in cm^{-1}					
1	460	440	450	451	441	Si-O-Si bending vibration Symm-Stretch of Si-O-Si
2	560	550	560	560	548	Metal-oxygen (Fe-O) vibrational mode
3	711	710	704	707	741	Mn-O-Mn stretching mode
4	1014	981	1012	1009	982	Si-O-Si asymm-stretch in SiO$_4$ group

The peaks indicating the bending vibration and asymmetric stretching vibration of Si-O-Si group suggests the formation of glass, while the stretching vibration of Mn-O-Mn indicates the presence of metal-oxygen bonds. However, the bands associated with Fe_2O_3 were not observed in the current glasses. This absence could be due to a combination of Fe^{2+} and Fe^{3+} states within the glass matrix. Additionally, the infrared data supports the likelihood of a silica glass framework forming.

41

4.4 Raman Spectroscopy

Raman analysis were done on the prepared glass samples by using Horiba raman spectrometer , the prepared glass samples were directly analyzed using laser light of 532 nm in the range of 200 to 1200 cm^{-1}. A broad peak was seen to be noticed at 635cm^{-1}which is ascribed to the Si-O-Si bending vibration group, peak at 935cm^{-1} which is in between 800-1150 cm^{-1} is associated to Si-O-Si stretching vibration bonds in the silica tetrahedrdon with a different number of Non-bridging oxygen, peak between 850-860 cm^{-1} can be ascribed to monomer SiO_4^{4-} with 4 NBOs.(Bellucci, Bolelli, Cannillo, Cattini, & Sola, 2011)
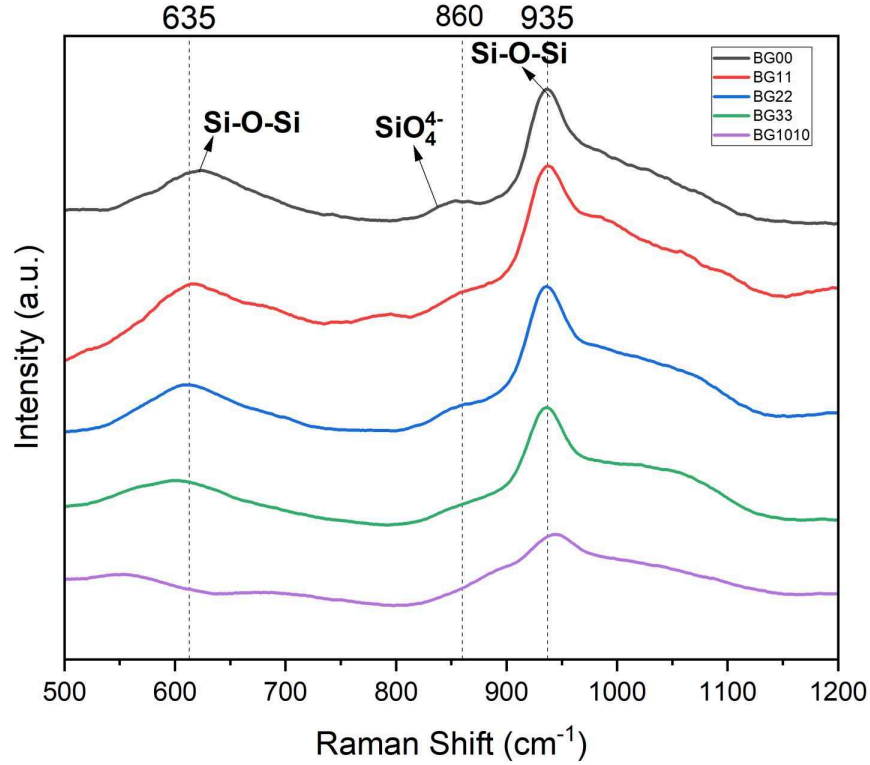
Figure 4.3: Raman Spectra of as-prepared Samples

Silicon-oxygen tetrahedra with various numbers of bridging oxygen atoms are the fundamental structural blocks of silicate glasses. The silicon oxygen tetrahedra are called Q^n units where n is the number of the bridging oxygen atoms per SiO_4 tetrahedron ranging from 0 to 4. (Bellucci et al., 2011).
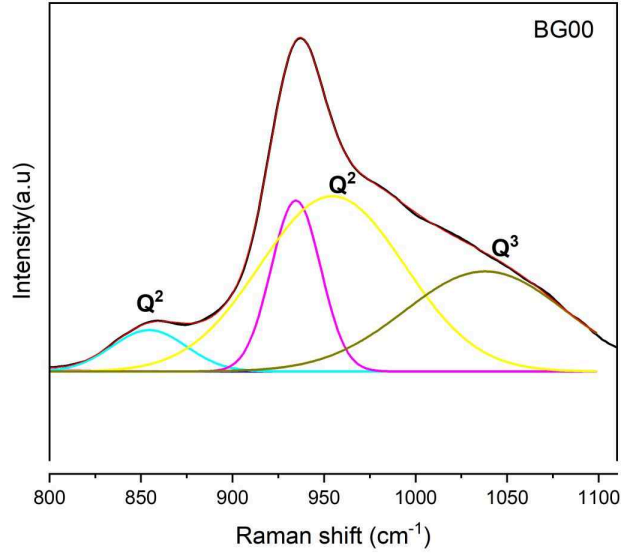
Figure 4.4: Deconvoluted peaks of BG00 sample
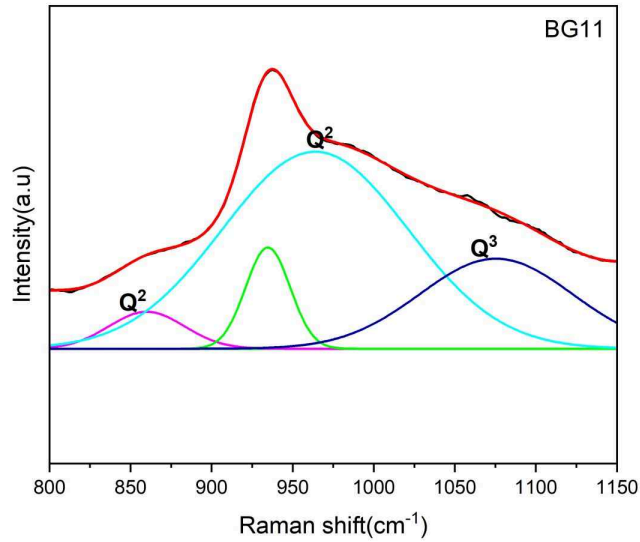
Figure 4.5: Deconvoluted peaks of BG11 sample
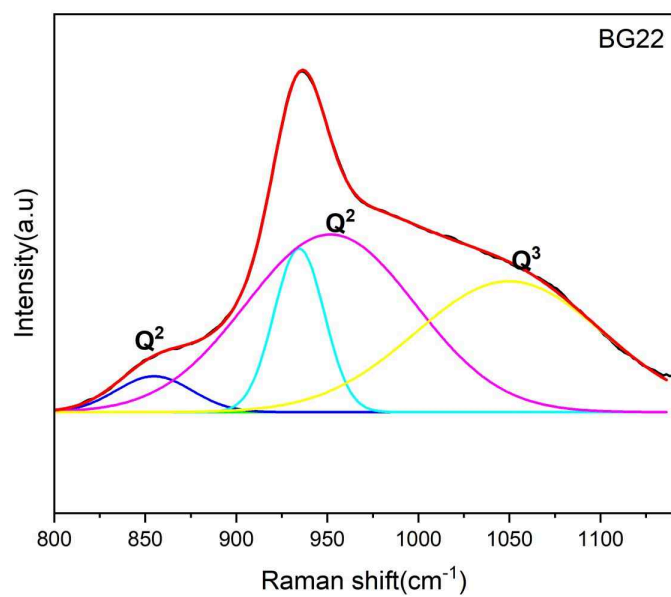
Figure 4.6: Deconvoluted peaks of BG22 sample
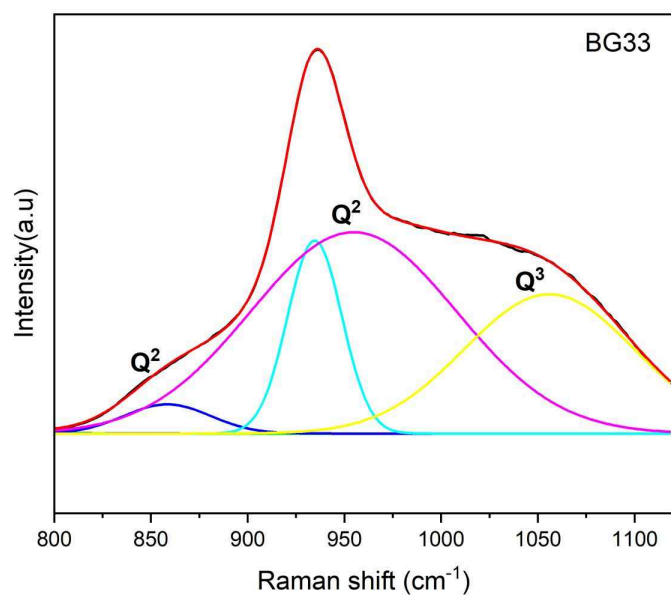
Figure 4.7: Deconvoluted peaks of BG33 sample
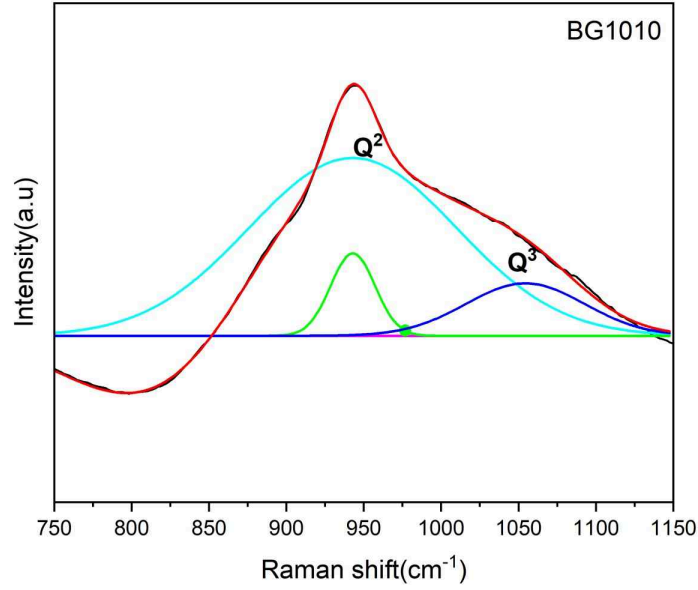
Figure 4.8: Deconvoluted peaks of BG1010 sample

Fig (4.4,4.5,4.6,4.7,4.8) shows the Deconvolution of Raman spectra in various Gaussian band and the peaks corresponding to Q^n that is Q^2 having 2 NBOs and Q^3 having 1 NBO which was noticed for all the samples.

For BG00,BG11,BG22 and BG33 samples two Q^2 peaks were seen close to 850 and 950 cm^{-1} respectively, while a single peak Q^3 was noticed between 1050-1080 cm^{-1}. BG1010 sample showed only two peaks one for Q^2 at 950cm^{-1} and another for Q^3 at 1050cm^{-1}.(Parkinson et al., 2008). After doing deconvolution of Raman spectra , it was observed that silicon network was desrupted by network modifier and doping of MnO_2 and Fe_2O_3 effects the structural properties of glass network.

4.5 UV-VISIBLE Spectroscopy

4.5.1 Optical absorption spectra

UV-Visible absorption spectra of these glasses were studied using a Shimadzu UV-2401PC spectrophotometer. The instrument covers a range of 200 to 800 nm and uses deuterium lamp as a source of UV light (200 to 400 nm) while tungsten-halogen lamp for the visible range (400 to 800 nm). The UV Visible absorbance spectra of prepared glasses doped with Fe_2O_3 is shown in figure (4.9). Each sample displays a singular, expansive absorption band with its peak near a wavelength of approximately 250 nm. As the proportion of iron within the samples rises, there is increase in absorption. Moreover, a shift towards longer wavelengths, or a 'red shift,' is observed with increasing iron levels. This phenomenon is likely due to presence of non-bridging oxygens (NBOs) resulting from the addition of iron oxide, which in turn promotes electron excitation from the more ionic NBOs compared to the less ionic bridging oxygens (BOs).
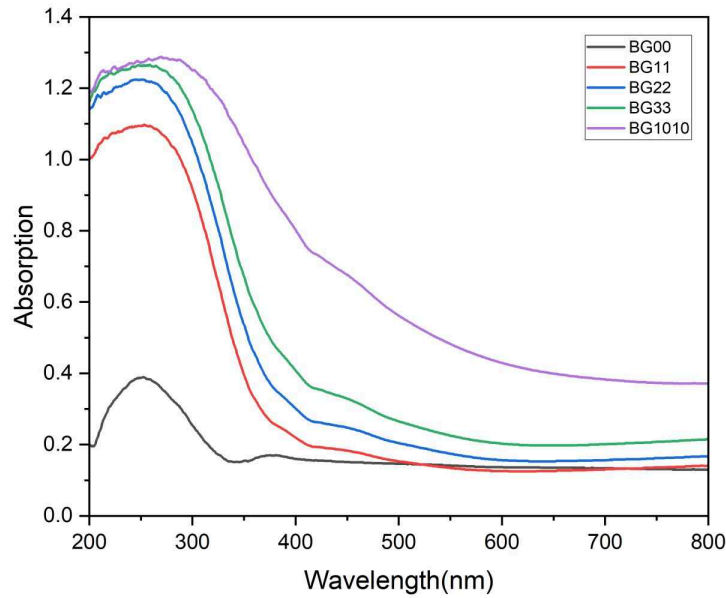
Figure 4.9: Absorption spectra of as-prepared Samples

4.5.2 Optical Band gap and Refractive Index

Optical band gap of glasses were calculated using UV-visible data from Tauc's plot. According to which the optical band gap was calculated using the formula:

$$(\alpha h\nu)^\gamma = A(h\nu - E_g)$$

Where:

α : Absorption coefficient, h : Planck's Constant, ν : Photon's frequency,

A : Proportionately constant, E_g : Band gap energy ,

γ : Nature of electron's transition , When:

$$\gamma = 2, \text{ it is direct allowed transition}$$
$$\gamma = \frac{1}{2}, \text{ it is indirect allowed transition}$$
$$\gamma = \frac{2}{3}, \text{ it is direct forbidden transition}$$
$$\gamma = \frac{1}{3}, \text{ it is indirect forbidden transition}$$

The allowed transition dominates over the basic absorption processes, giving either direct or indirect transition. Thus, the basic procedure for a Tauc's analysis is to acquire optical absorbance data for a sample that spans the range of energies from below the Bandgap transition to above it. We plot $(\alpha h\nu)^\gamma$ versus $(h\nu)$ to test whether $\gamma = 2$ or $\gamma = \frac{1}{2}$ provides a better fit. Hence, $(\alpha h\nu)^2$ was plotted against $(h\nu)$, and the obtained linearity in the curve was made to intersect on the x-axis, and $(\alpha\nu)^2$ was made zero to get the optical band gap. Optical band gap obtained for all glass samples were seen in the Fig 4.10 , The optical band gap for all the samples was plotted and was tabulated in Table 4.3 , it was found that as the iron content increases the optical band gap lowers, which in turn increases the conductivity in the sample.

(a) BG00   (b) BG11   (c) BG22

(d) BG33   (e) BG1010
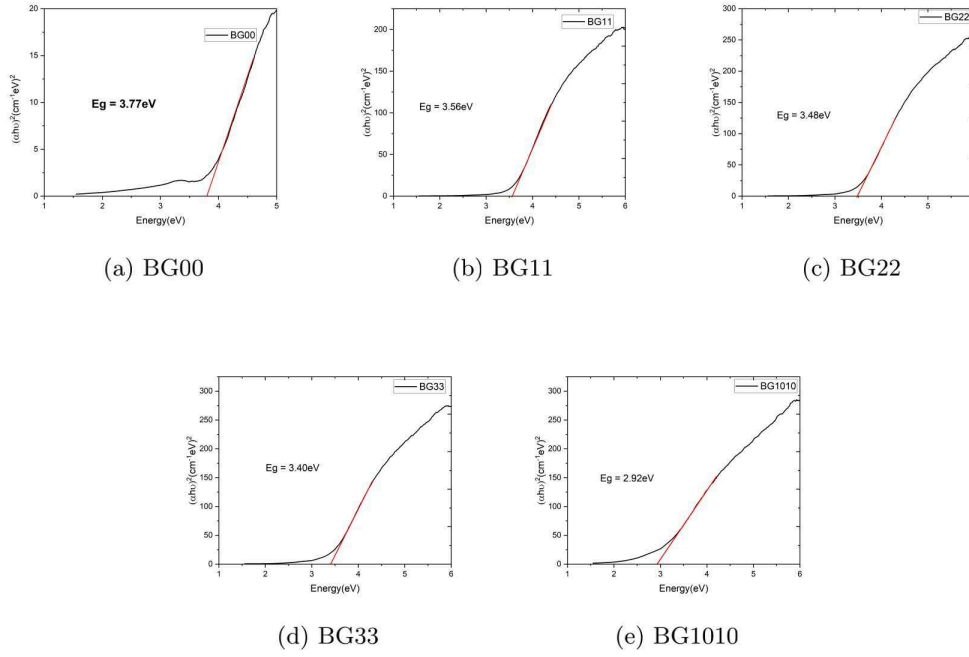
Figure 4.10: Optical Band gaps of as-prepared Samples

Using the calculated optical band gap, the refractive index for all the glasses were found using(Obayes, Wagiran, Hussin, & Saeed, 2016)

$$\frac{n^2 - 1}{n^2 + 2} = 1 - \sqrt{\frac{Eg}{20}}$$

where, Eg = Bandgap of samples and n = Refractive index

The refractive index for all the glass sample has been showed in Table 4.3 , It showed a increasing trend in the refractive index with the increase in iron content and this variation can be due to increase in NBOs because they create a less tightly packed network structure, allowing more polarizability within the material. This increased polarizability can lead to a higher refractive index.(M.Vinoda Rani, 2023)

Table 4.3: Bandgap and Refractive Index of as-prepared glasses

Sample	Bandgap(Eg)	Refractive Index (n)
BG00	3.77	2.22
BG11	3.56	2.26
BG22	3.48	2.27
BG33	3.4	2.30
BG1010	2.92	2.42

4.6 SEM Analysis

The morphology characterization on the samples was done using ZEISS Evo 18 scanning electron microscope.For all the samples homogenous surfaces including random size particles were noticed.
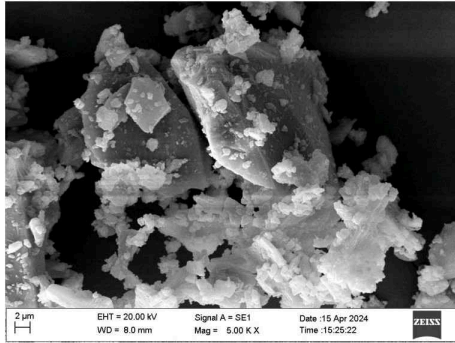
(a) BG00
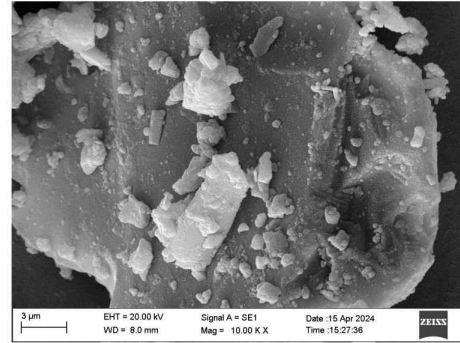
(b) BG11
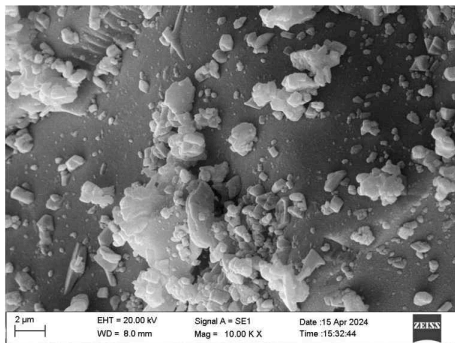
(c) BG22
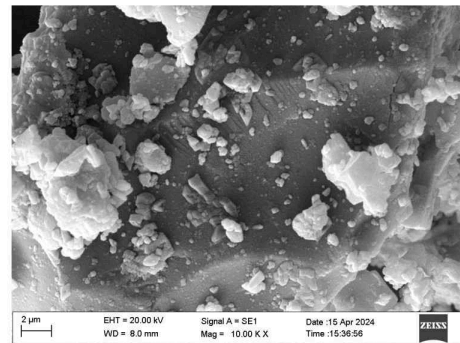
(d) BG33
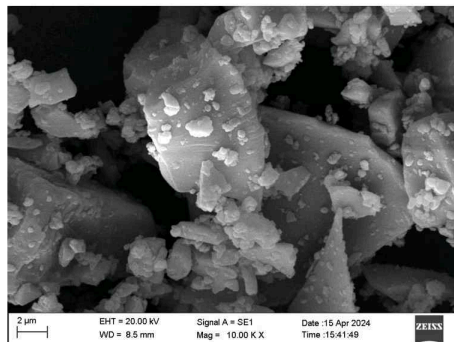
(e) BG1010

Figure 4.11: SEM micrographs of as-prepared samples

4.7 In-Vitro Test

4.7.1 Hydroxyapatite (Hap) peaks detection using XRD

The XRD diffraction patterns of the glass samples were examined before and after immersion in SBF solution for 7, 14, and 20 days Fig(4.12,4.13,4.14,4.15,4,16) represents all the glass samples,Prior to immersion, the BG00 sample exhibited a broad hump. After 7 days, characteristic peaks near 29°and 45°were observed, confirming the formation of an HAp layer, as reported by Lara Ochoa et al. After 14 days, there was minimal change in the peaks, which remained at the same 2θ angles. By day 20, a sharp peak appeared at 31.78°(211)(Palakurthy, K., Samudrala, & P., 2019), with additional peaks at 29°, 45.32°, and 48.59°.(Lara Ochoa, Ortega, & Guerrero-Beltrán, 2021)

In contrast, the BG11 sample showed no peaks after 7 days, but developed peaks near 29°and 48.59°after 14 days, and similar peaks along with the sharp peak at 31.78°(211) after 20 days. BG22 did not exhibit any peaks after 7 days, but showed a single peak near 29°after 14 days, followed by the appearance of the sharp peak at 31.78°(211) and others near 29°and 45.32°after 20 days. BG33 displayed a diffraction pattern similar to BG22 after 20 days, with an additional peak close to 45.32°after 14 days and one near 29°after 7 days.Lastly, the BG1010 sample lacked peaks after 7 and 14 days, but displayed a sharp peak at 31.78°(211)(Palakurthy et al., 2019) and another close to 45.32°after 20 days.(Lara Ochoa et al., 2021).

This all peaks are confirmed for Hydroxyapatite($Ca_{10}(PO_4)_6(OH)_2$) using (JCPDS 00-0009-0432) card number(Lara Ochoa et al., 2021).Out of all samples BG00 sample showed up better bioactivity as it formed Hap layer immediately after 7 days of SBF immersion while BG1010 took longer time and formed Hap layer after 20 days.
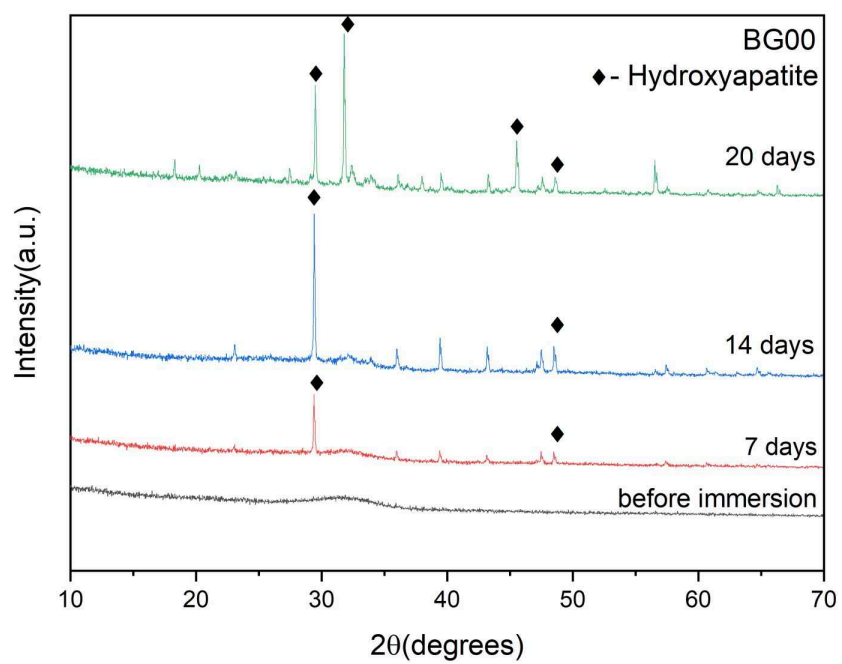
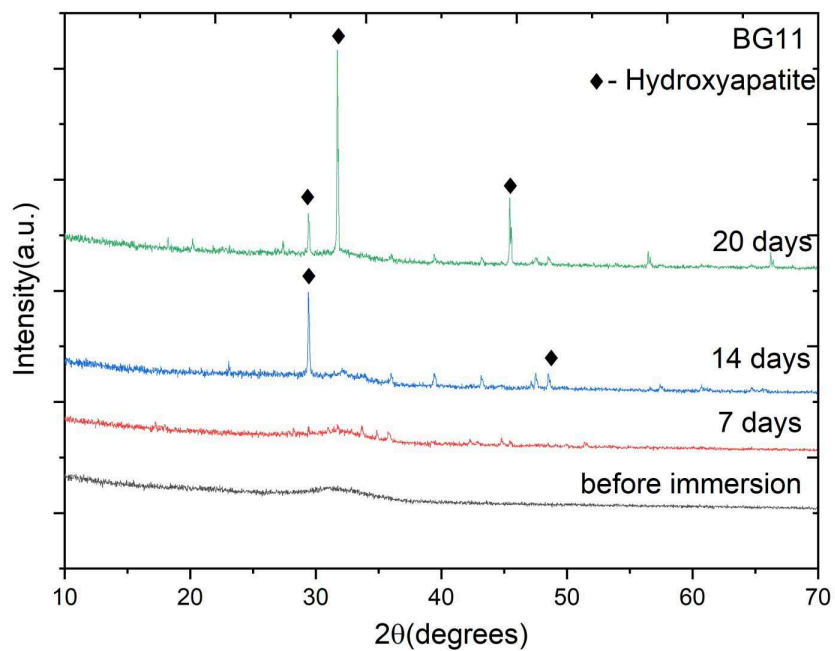Figure 4.12: HAp peaks of BG00 sample
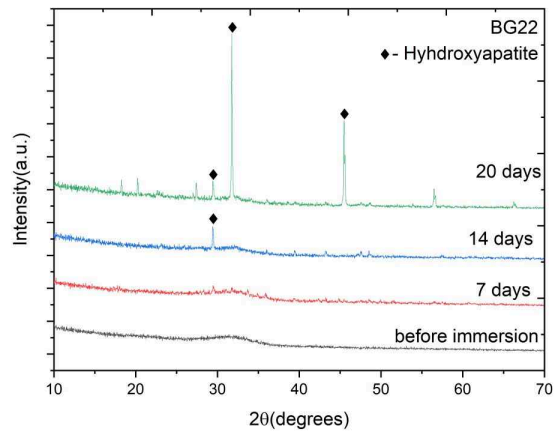

Figure 4.13: HAp peaks of BG11 sample
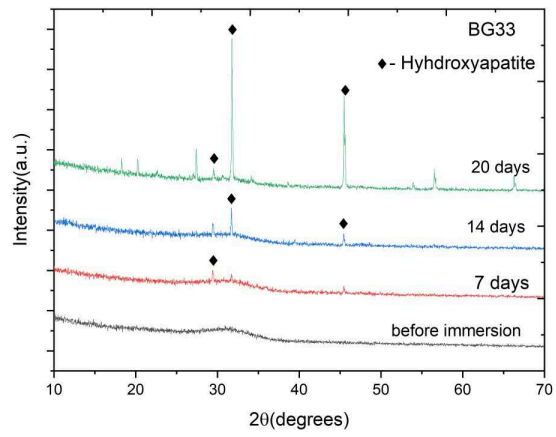
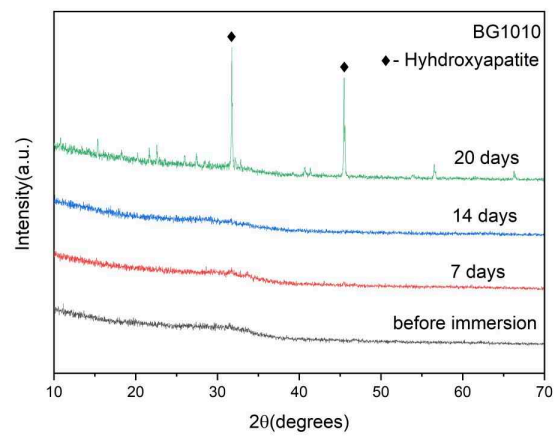Figure 4.14: HAp peaks of BG22 sample


Figure 4.15: HAp peaks of BG33 sample

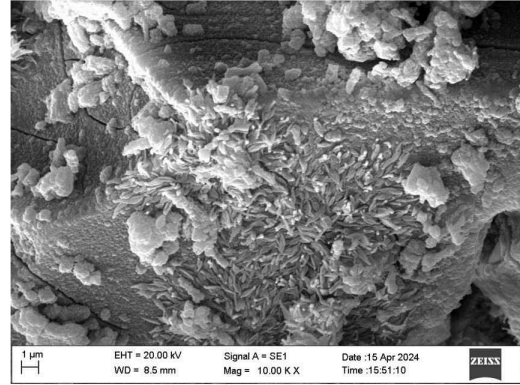
Figure 4.16: HAp peaks of BG1010 sample

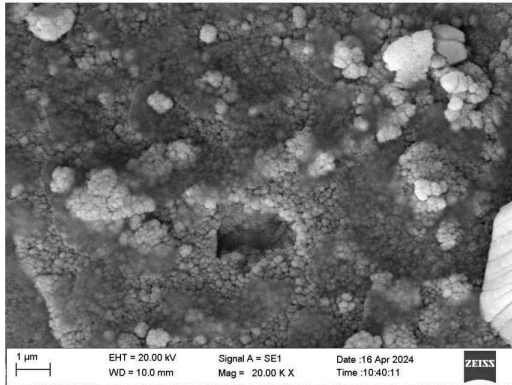### 4.7.2   Hydroxyapatite (Hap) Surface detection using SEM

For In-vitro test The glass samples were analysed and compared based on before and after immersion in SBF for 7 , 14 and 20 days , After immersion in SBF specific change in surface of the samples were noticed which are shown in Fig(4.17,4.18,4.19,4.20,4.21)
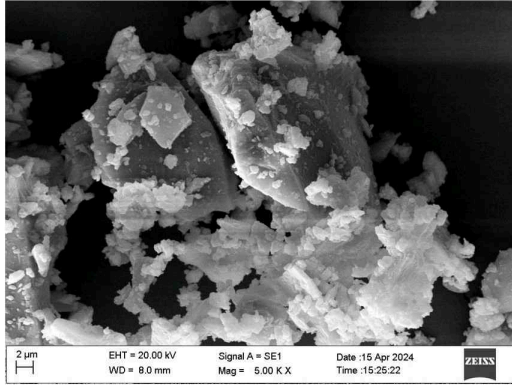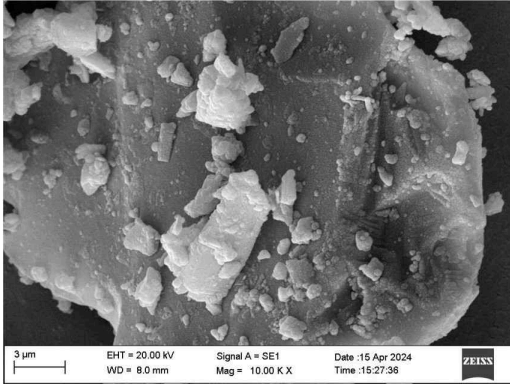

(a) Before immersion in SBF

(b) After 7 days of SBF immersion
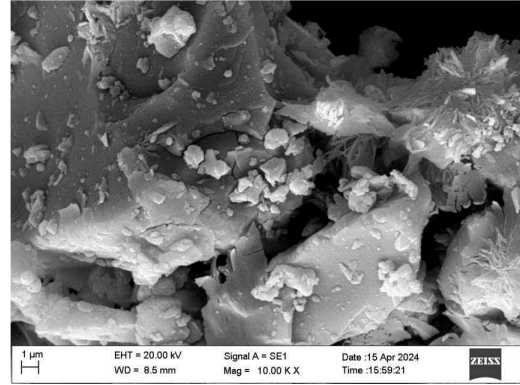

(c) After 14 days of SBF immersion
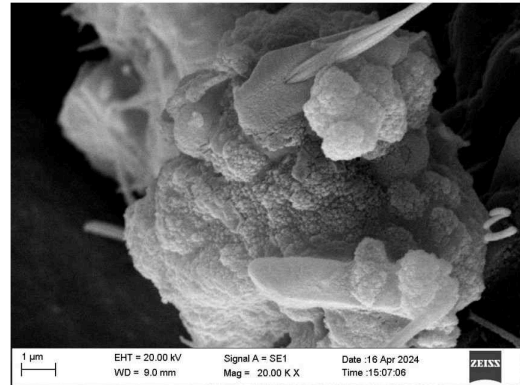
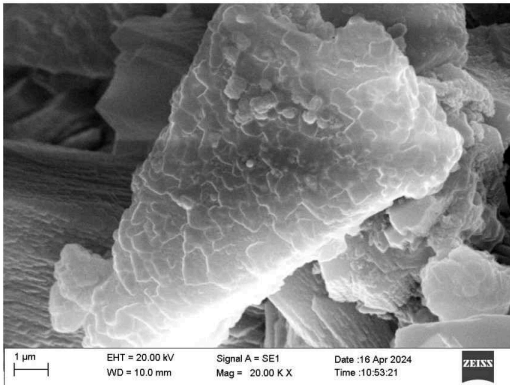(d) After 20 days of SBF immersion

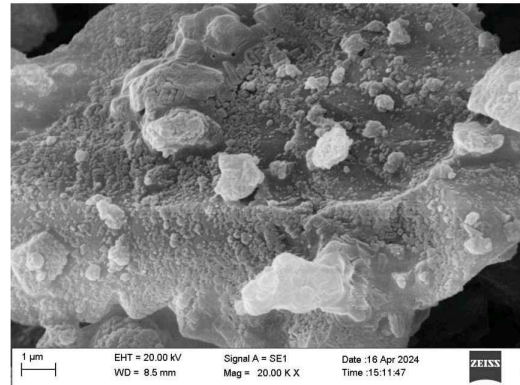Figure 4.17: HAp Surface detection of BG00 sample

(a) Before immersion in SBF
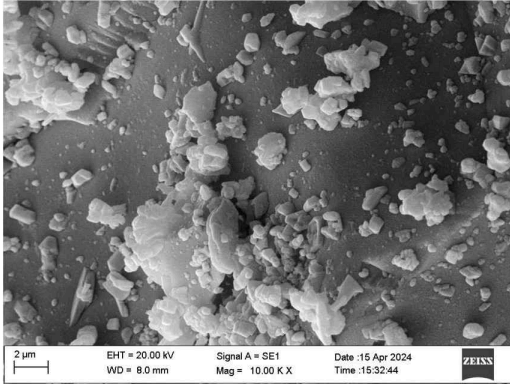

(b) After 7 days of SBF immersion

(c) After 14 days of SBF immersion

(d) After 20 days of SBF immersion

Figure 4.18: HAp Surface detection of BG11 sample

(a) Before immersion in SBF

(b) After 7 days of SBF immersion

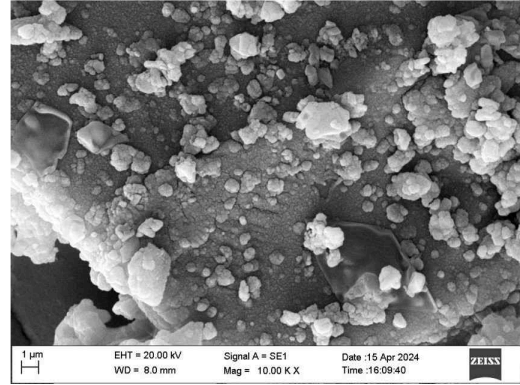(c) After 14 days of SBF immersion

(d) After 20 days of SBF immersion

Figure 4.19: HAp Surface detection of BG22 sample

(a) Before immersion in SBF

(b) After 7 days of SBF immersion

(c) After 14 days of SBF immersion

(d) After 20 days of SBF immersion

Figure 4.20: HAp Surface detection of BG33 sample

(a) Before immersion in SBF

(b) After 7 days of SBF immersion

(c) After 14 days of SBF immersion
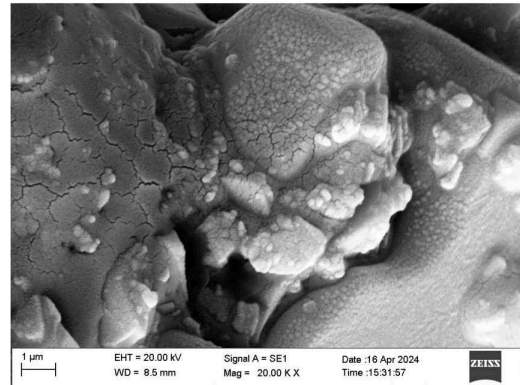
(d) After 20 days of SBF immersion

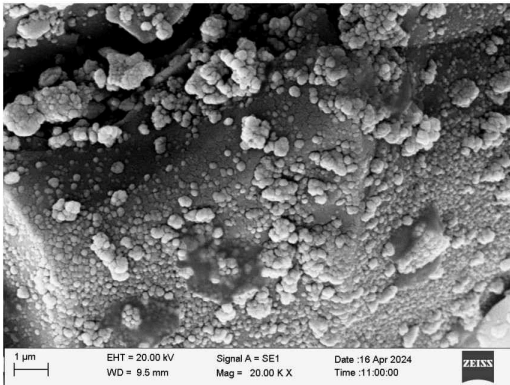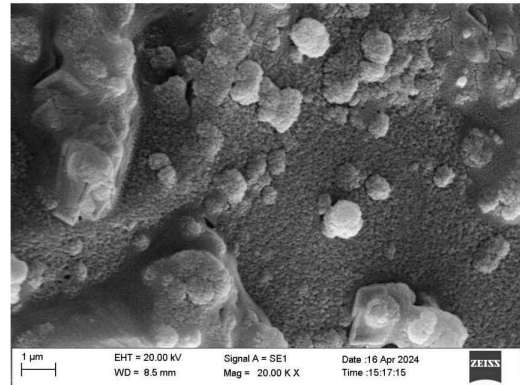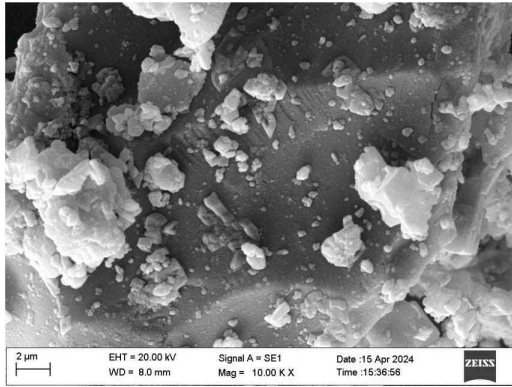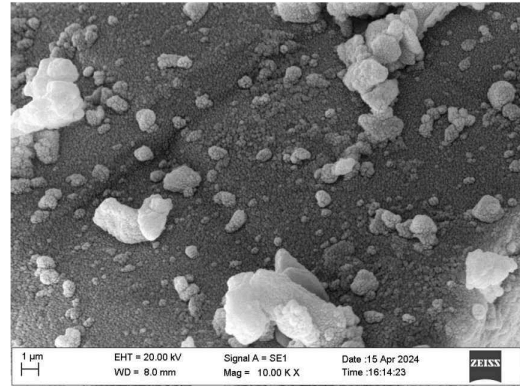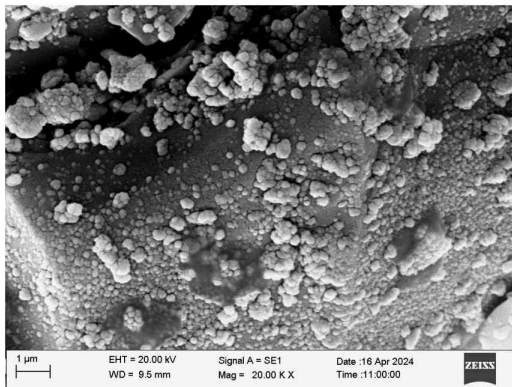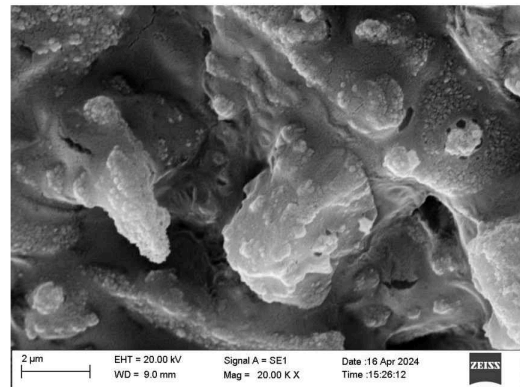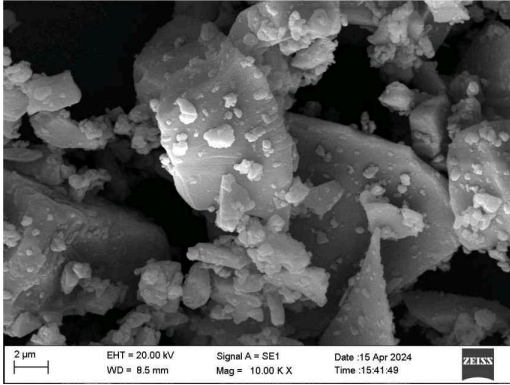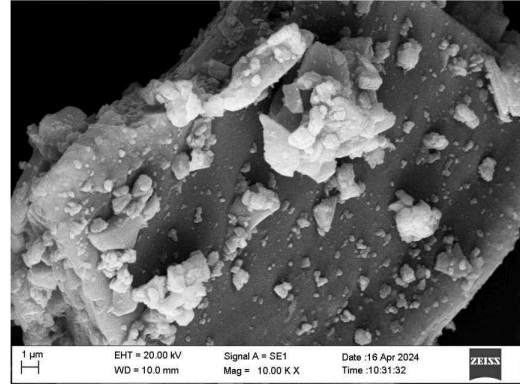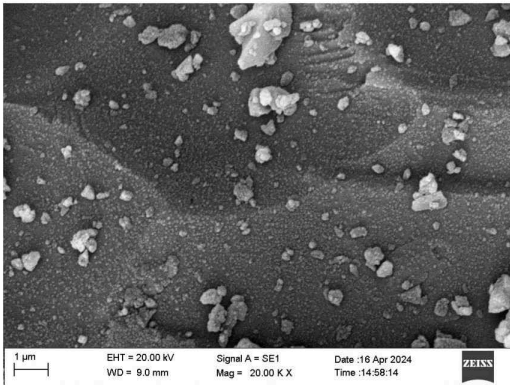Figure 4.21: HAp Surface detection of BG1010 sample

4.8   Conclusion

Our study successfully synthesized and characterized Bioactive Silicate glasses doped with transition metals MnO_2 and Fe_2O_3 using the melt-quenching method. Through various analysis , which included XRD, FTIR, Raman, UV-VIS, and SEM, we studied the physical, optical, and structural properties of these glasses. Our findings revealed that the incorporation of MnO_2 and Fe_2O_3 resulted in increased glass density without compromising its amorphous nature, making them effective intermediates in glass formation.

In-vitro studies conducted in simulated body fluid demonstrated the bioactivity of the glasses, with differing rates of Hydroxyapatite (HAp) layer formation observed for different compositions using XRD and SEM. Moreover, UV-VIS analysis revealed a correlation between Fe_2O_3 content with optical absorbance, refractive index, and bandgap. Overall, our study highlights the potential of $(MnO_2 and Fe_2O_3)$ doped bioactive silicate glasses for various biomedical applications, owing to their favorable physical, optical, and bioactive properties.

4.9 Scope For Future Work

The composition of glass containing $MnO_2 - Fe_2O_3$ can be adjusted with varying proportions and can be studied for their structural properties and Bioactivity.The prepared glass samples can be analyzed for magnetic properties using Vibrating Scanning Magnetometer or SQUID to study M-H loops and hysteresis losses , providing insights into whether the samples are suitable for hyperthermia treatment of cancer or not.

Additionally, Fourier Transform Infrared (FTIR) analysis can be conducted on the samples after immersion in simulated body fluid (SBF) to assess their bioactivity. Cytotoxicity studies and One could also explore how the effect of prolonged exposure to simulated body fluid (SBF) impacts both the magnetic properties and the durability of the resulting Hydroxyapatite (HAp) layer.

References

Akash, M. S. H., & Rehman, K. (2020). Ultraviolet-visible (uv-vis) spectroscopy. In *Essentials of pharmaceutical analysis* (pp. 29–56). Singapore: Springer Nature Singapore. Retrieved from `https://doi.org/10.1007/978-981-15-1547-7_3` doi: 10.1007/978-981-15-1547-7_3

Australian Microscopy and Microanalysis Research Facility. (accessed online on 3-5-2018). *MyScope - Training for Advanced Research.* Retrieved from `http://www.ammrf.org.au/myscope/sem/background/`

Baino, F., Fiume, E., Miola, M., Leone, F., Onida, B., Laviano, F., . . . Verné, E. (2018). Fe-doped sol-gel glasses and glass-ceramics for magnetic hyperthermia. *Materials*, *11*(1). Retrieved from `https://www.mdpi.com/1996-1944/11/1/173` doi: 10.3390/ma11010173

Bellucci, D., Bolelli, G., Cannillo, V., Cattini, A., & Sola, A. (2011). In situ raman spectroscopy investigation of bioactive glass reactivity: Simulated body fluid solution vs tris-buffered solution. *Materials Characterization*, *62*(10), 1021-1028. Retrieved from `https://www.sciencedirect.com/science/article/pii/S1044580311001719` doi: https://doi.org/10.1016/j.matchar.2011.07.008

Bizari, D., Yazdanpanah, A., & Moztarzadeh, F. (2020). Bao–fe2o3 containing bioactive glasses: A potential candidate for cancer hyperthermia. *Materials Chemistry and Physics*, *241*, 122439. Retrieved from `https://www.sciencedirect.com/science/article/pii/S0254058419312532` doi: https://doi.org/10.1016/j.matchemphys.2019.122439

Brown, M. E. (1988). Differential thermal analysis (dta) and differential scanning calorimetry (dsc). In *Introduction to thermal analysis: Techniques and applications* (pp. 23–49). Dordrecht: Springer Netherlands. Retrieved from `https://doi.org/10.1007/978-94-009-1219-9_4` doi: 10.1007/978-94-009-1219-9_4

Bumbrah, G. S., & Sharma, R. M. (2016). Raman spectroscopy â€" basic principle, instrumentation and selected applications for the characterization of drugs of abuse. *Egyptian Journal of Forensic Sciences*, *6*(3), 209-215. Retrieved from `https://www.sciencedirect.com/science/article/pii/S2090536X15000477` doi: https://doi.org/10.1016/j.ejfs.2015.06.001

Chemical vapor deposition. (2008). In *The materials science of semiconductors* (pp. 573–609). Boston, MA: Springer US. Retrieved from `https://doi.org/10.1007/978-0-387-68650-9_12` doi: 10.1007/978-0-387-68650-9_12

Chopinet, M.-H. (2019). The history of glass. In J. D. Musgraves, J. Hu, & L. Calvez (Eds.), *Springer handbook of glass* (pp. 1–47). Cham: Springer International Publishing. Retrieved from `https://doi.org/10.1007/978-3-319-93728-1_1` doi: 10.1007/978-3-319-93728-1_1

Danewalia, S., & Singh, K. (2021). Bioactive glasses and glass–ceramics for hyperthermia treatment of cancer: state-of-art, challenges, and future perspectives. *Materials Today Bio*, *10*, 100100. Retrieved from `https://www.sciencedirect.com/science/article/pii/S2590006421000089` doi: https://doi.org/10.1016/j.mtbio.2021.100100

Danewalia, S. S., & Singh, K. (2016). Magnetic and bioactive properties of mno2/fe2o3 modified na2o-cao-p2o5-sio2 glasses and nanocrystalline glass-ceramics. *Ceramics International*, *42*(10), 11858-11865. Retrieved from `https://www.sciencedirect.com/science/article/pii/S0272884216305144` doi: https://doi.org/10.1016/j.ceramint.2016.04.108

Daéid, N. (2005). Forensic sciences — systematic drug identification. In P. Worsfold, A. Townshend, & C. Poole (Eds.), *Encyclopedia of analytical science (second edition)* (Second Edition ed., p. 471-480). Oxford: Elsevier. Retrieved from `https://www.sciencedirect.com/science/article/pii/B0123693977001977` doi: https://doi.org/10.1016/B0-12-369397-7/00197-7

Dziadek, M., Zagrajczuk, B., Menaszek, E., Wegrzynowicz, A., Pawlik, J., & Cholewa-Kowalska, K. (2016). Gel-derived sio2–cao–p2o5 bioactive glasses and glass-ceramics modified by sro addition. *Ceramics International*, *42*(5), 5842-5857. Retrieved from `https://www.sciencedirect.com/science/article/pii/S0272884215024268` doi: https://doi.org/10.1016/j.ceramint.2015.12.128

The editors of encyclopaedia. "obsidian". (2024). *Encyclopedia Britannica*.

Elliot, S. R., & Download, F. (1985). Physics of amorphous materials by s. r. elliott.. Retrieved from `https://api.semanticscholar.org/CorpusID:97309714`

Giechaskiel, B., & Clairotte, M. (2021). Fourier transform infrared (ftir) spectroscopy for measurements of vehicle exhaust emissions: A review. *Applied Sciences*, *11*(16). Retrieved from `https://www.mdpi.com/2076-3417/11/16/7416` doi: 10.3390/app11167416

Hastuti, E., Subhan, A., Amonpattaratkit, P., Zainuri, M., & Suasmoro, S. (2021, 02). The effects of fe-doping on mno 2 : phase transitions, defect structures and its influence on electrical properties. *RSC Advances*, *11*, 7808-7823. doi: 10.1039/D0RA10376D

Holder, C. F., & Schaak, R. E. (2019). Tutorial on powder x-ray diffraction for characterizing nanoscale materials. *ACS Nano*, *13*(7), 7359-7365. Retrieved from `https://doi.org/10.1021/acsnano.9b05157` (PMID: 31336433) doi: 10.1021/acsnano.9b05157

JONES, J. R. (2008). 12 - bioactive glass. In T. Kokubo (Ed.), *Bioceramics and their clinical applications* (p. 266-283). Woodhead Publishing. Retrieved from `https://www.sciencedirect.com/science/article/pii/B9781845692049500120` doi: https://doi.org/10.1533/9781845694227.2.266

Kokubo, T., & Takadama, H. (2007). Simulated body fluid (sbf) as a standard tool to test the bioactivity of implants. In *Handbook of biomineralization* (p. 97-109). John Wiley Sons, Ltd. Retrieved from `https://onlinelibrary.wiley.com/doi/abs/10.1002/9783527619443.ch51` doi: https://doi.org/10.1002/9783527619443.ch51

Lara Ochoa, S., Ortega, W., & Guerrero-Beltrán, E. (2021, 10). Hydroxyapatite nanoparticles in drug delivery: Physicochemistry and applications. *Pharmaceutics*, *13*. doi: 10.3390/pharmaceutics13101642

M., S., S, M., & Kumari S, S. (2021, 03). Highlights of spectroscopic analysis – a review. *International Journal of pharma and Bio Sciences*, *11*, 136-145. doi: 10.22376/ijpbs/lpr.2021.11.2.P136-145

Mohammed, A., & Abdullah, A. (2019, 01). Scanning electron microscopy (sem): A review..

M.Vinoda Rani, A. S. C. S. N. R., Raju Vaddiraju. (2023). The role of nbos on optical and physical properties of na2o added sb2o3-zno-b2o3 glasses. *IOSR Journal of Applied Physics (IOSR-JAP)*, *15*(2), 55–60.

Obayes, H. K., Wagiran, H., Hussin, R., & Saeed, M. (2016). Strontium ions concentration dependent modifications on structural and optical features of li4sr(bo3)3 glass. *Journal of Molecular Structure*, *1111*, 132-141. Retrieved from `https://www.sciencedirect.com/science/article/pii/S0022286016300886` doi: https://doi.org/10.1016/j.molstruc.2016.01.088

of Encyclopaedia Britannica, T. E. (2023, March 31). *X-ray diffraction.* `https://www.britannica.com/science/X-ray-diffraction`. (Encyclopedia Britannica)

Omidian, S., Haghbin Nazarpak, M., Bagher, Z., & Moztarzadeh, F. (2022). The effect of vanadium ferrite doping on the bioactivity of mesoporous bioactive glass-ceramics. *RSC Adv.*, *12*, 25639-25653. Retrieved from `http://dx.doi.org/10.1039/D2RA04786A` doi: 10.1039/D2RA04786A

Palakurthy, S., K., V. G. R., Samudrala, R. K., & P., A. A. (2019). In vitro bioactivity and degradation behaviour of -wollastonite derived from natural waste. *Materials Science and Engineering: C*, *98*, 109-117. Retrieved from `https://www.sciencedirect.com/science/article/pii/S0928493118312967` doi: https://doi.org/10.1016/j.msec.2018.12.101

Parkinson, B., Holland, D., Smith, M., Larson, C., Doerr, J., Affatigato, M., ... Scales, C. (2008). Quantitative measurement of q3 species in silicate and borosilicate glasses using

raman spectroscopy. *Journal of Non-Crystalline Solids*, *354*(17), 1936-1942. Retrieved from `https://www.sciencedirect.com/science/article/pii/S0022309307012938` doi: https://doi.org/10.1016/j.jnoncrysol.2007.06.105

Pasek, M. A., Block, K., & Pasek, V. (2012). Fulgurite morphology: a classification scheme and clues to formation. *Contributions to Mineralogy and Petrology*, *164*(3), 477-492. (Communicated by C. Ballhaus.) doi: 10.1007/s00410-012-0753-5

S a, P. (2021, 10). Squid magnetometer -a study.
doi: 10.13140/RG.2.2.17984.66564

Singh, R. K., & Srinivasan, A. (2011). Magnetic properties of bioactive glass-ceramics containing nanocrystalline zinc ferrite. *Journal of Magnetism and Magnetic Materials*, *323*(3), 330-333. Retrieved from `https://www.sciencedirect.com/science/article/pii/S0304885310006724` doi: https://doi.org/10.1016/j.jmmm.2010.09.029

Zhou, W., Apkarian, R., Wang, Z. L., & Joy, D. (2007). Fundamentals of scanning electron microscopy (sem). In W. Zhou & Z. L. Wang (Eds.), *Scanning microscopy for nanotechnology: Techniques and applications* (pp. 1–40). New York, NY: Springer New York. Retrieved from `https://doi.org/10.1007/978-0-387-39620-0_1` doi: 10.1007/978-0-387-39620-0_1

Žaludová, M., Smetana, B., Zlá, S., Dobrovska, J., Gryc, K., Michalek, K., & Dudek, R. (2012, 01). Study of dta method experimental conditions and of their influence on obtained data of metallic systems. *METAL 2012 - Conference Proceedings, 21st International Conference on Metallurgy and Materials*.

(S. Danewalia & Singh, 2021) (Pasek et al., 2012) ("The Editors of Encyclopaedia. "obsidian"", 2024) (Chopinet, 2019) (Elliot & Download, 1985) ("Chemical Vapor Deposition", 2008) (M., S, & Kumari S, 2021) (Holder & Schaak, 2019) (Daéid, 2005) (Giechaskiel & Clairotte, 2021) (Bumbrah & Sharma, 2016) (Akash & Rehman, 2020) (Zhou et al., 2007) (Mohammed & Abdullah, 2019) (Australian Microscopy and Microanalysis Research Facility, accessed online on 3-5-2018) (S a, 2021) (Žaludová et al., 2012) (Brown, 1988) (M.Vinoda Rani, 2023) (Bizari et al., 2020) (Omidian et al., 2022) (Hastuti et al., 2021) (JONES, 2008) (Baino et al., 2018) (S. S. Danewalia & Singh, 2016) (Dziadek et al., 2016) (Singh & Srinivasan, 2011) (Obayes et al., 2016) (Kokubo & Takadama, 2007) (of Encyclopaedia Britannica, 2023)